Relation between continental strike-slip earthquake segmentation and thickness of the crust

Yann Klinger

JOURNAL OF GEOPHYSICAL RESEARCH, VOL. 115, B07306, doi:10.1029/2009JB006550, 2010

Relation between continental strike-slip earthquake segmentation and thickness of the crust

Yann Klinger[1,2]

Received 17 April 2009; revised 1 February 2010; accepted 25 February 2010; published 16 July 2010.

[1] High-resolution maps of large continental strike-slip earthquake surface ruptures show that they are formed of fault segments. These segments are bounded by fault bends, step overs, or combinations of the two. The lowest limit in size for such segments may not be relevant in the understanding of earthquake mechanics, as it pertains to the granular properties of fault zones. The maximum limit in segment length, however, is important as it is directly relates to the maximum extent of seismic rupture. To measure the length of the segments, a new quantitative method based on piecewise linear fitting is developed and is used to automatically retrieve segments from earthquake rupture maps. Next, this approach is tested against a set of ten continental strike-slip earthquake ruptures derived from similar, high quality maps. The test suggests that segments have a maximum length of ~18 km, independent of regional tectonic setting. Slip-inversions for earthquakes, based on seismological and/or geodetic data, most often are not unique and can show some variability even for one particular event. Some basic characteristics, however, such as total moment release or general source geometry, seem to persist that are relevant to earthquake mechanics. Measurements of the maximum horizontal extent of individual slip-patches derived from seismic source inversion for strike-slip ruptures show that their strike dimension does not increase infinitely with magnitude, but instead reaches a maximum value of ~25 km. These two independent lines of observations, complemented by earlier data and analog experiments, suggest that it is the thickness of the seismogenic crust that controls the structural scaling of the length of seismic segments, and that it is independent of the ultimate size of individual earthquakes.

Citation: Klinger, Y. (2010), Relation between continental strike-slip earthquake segmentation and thickness of the crust, *J. Geophys. Res.*, *115*, B07306, doi:10.1029/2009JB006550.

1. Introduction

[2] Coseismic continental strike-slip ruptures are usually segmented, with segments separated by step over and fault bends. It has been shown that these step over and bends have a direct impact on the initiation locations and ends of earthquake ruptures [*King and Nabelek*, 1985; *Wesnousky*, 1988; *Knuepfer*, 1989; *Duan and Oglesby*, 2006; *Wesnousky*, 2006]. For example, the 1995, Mw7.1 Kobe earthquake, in Japan, appeared to nucleate at a fault segment boundary, and proceeded to propagate bilaterally [*Aochi et al.*, 2000]. The 2001, Mw7.8 Kokoxili earthquake, in Tibet, also started in a pull-apart basin and propagated bilaterally [*Klinger et al.*, 2005]. The dynamic propagation of the earthquake rupture is also directly affected by the geometry of the rupture [*Fliss et al.*, 2005; *Bhat et al.*, 2007; *Vallée et al.*, 2008], and the possible critical size for such geometric asperities to stop a rupture has been extensively investigated both from field observations [*Lettis et al.*, 2002; *Duman et al.*, 2005; *Wesnousky*, 2006; *Graymer et al.*, 2007] and rupture propagation modeling [*Harris and Day*, 1993, 1999; *Duan and Oglesby*, 2006]. Fault segmentation is an essential ingredient to define seismic cycle models and various scaling laws [*Schwartz and Coppersmith*, 1984; *Sieh*, 1996; *Weldon et al.*, 2004; *Manighetti et al.*, 2007]. The length of fault segments has, however, received little attention, although the length is a key parameter when designing rupture scenarios. Although it might be difficult to discern anything meaningful when one looks at surface ruptures at scales that are smaller than a few tens of meters, observations at the kilometric scale are pertinent. Here we investigate whether there is a maximum length for fault segments that participate in the control of the extent of earthquake rupture [*Stirling et al.*, 1996]. The upper limit for the segment length has long been intuitively associated with the thickness of the crust [*Scholz*, 1990, 1998], but that relationship has never been confirmed. Here, based on surface rupture maps and patterns of slip distribution derived from kinematic inversion of seismological and geodetic data, I suggest that for large continental strike-slip earthquakes, the length of a seismically rupturing segment is

[1]Institut de Physique du Globe Paris, CNRS, Paris, France.
[2]Also at Department of Earth and Planetary Sciences, Harvard University, Cambridge, Massachusetts, USA.

0148-0227/10/2009JB006550

Table 1. List of Earthquake Rupture Maps Used in This Study[a]

Name	Year	Magnitude	Total Rupture Length (km)	Number of Segments	Average Length of Segments (km)	Standard Deviation	Total Geologic Offset (km)
Owens Valley (United States)	1872	Mw 7.5–7.8	78	4	19.5	3.6	20
Haiyuan (China)	1920	Ms 8	250	11 (+2/−1)	22.6	3.9	125
Gobi-Altay (Mongolia)	1957	M 8.3	242	15 (+0/−2)	16.24	5.66	<20
Korizan (Iran)	1979	Mw 6.6	20	1	20	-	70–90
Superstition Hills (United States)	1987	M 6.6	18.6	2	9.3	0.7	≤24
Luzon (Philippine)	1990	Mw 7.8	>120	6 (+1/−0)	19	4.7	<200
Landers (United States)	1992	Mw 7.2	75	4 (+1/−0)	19	0.9	>40
Zirkuh (Iran)	1997	Mw 7.2	100	5	20.9	6	70–90
Hector Mine (United States)	1999	Mw 7.1	39	4 (+0/−1)	10.25	2.71	≤10
Kokoxili (China)	2001	Mw 7.8	430	14 (+0/−2)	15.3	2.99	150

[a]Total offset is indicated when available. References for each earthquake are cited in the text.

limited, and that the critical length scales with the thickness of the seismogenic crust and is independent of the geological context.

[3] In the first part of this paper, I discuss the availability and quality of rupture maps for large continental strike-slip earthquakes. Next, I describe an automatic method to determine the minimum number of fault segments needed to approximate an individual surface rupture. This method is tested on the detailed rupture maps of ten earthquakes with magnitudes that range between 6 and 8 to determine the possible segmentation of the surface rupture trace. This test shows that the average length of segments is 17.9 km ± 5.2 km for our data set. In the second part of this paper, for 17 continental strike-slip earthquakes and one oceanic strike-slip event (M. Mai, Database of finite-source rupture models, 2007, available at http://www.seismo.ethz.ch/srcmod/), slip maps derived from kinematic inversion of seismic waves and geodetic data have been analyzed to measure maximum horizontal length of slip patches. It shows that for each event, the maximum length of the largest slip patch is ~25 km. In the discussion section I show that such characteristic length for segments and slip patches can be related to previously published observations and analog experiments, and data collectively suggest a strong geometrical scaling between the thickness of the rupturing medium and the size of segments. Such scaling implies that despite some large scale smoothing of the fault with time, a specific level of segmentation is maintained as the fault evolves, related to the thickness of the crust. Consequently, fault segmentation must be considered when modeling earthquake rupture and strong ground motion.

2. Surface Rupture Data

2.1. Surface Rupture Segmentation

[4] To characterize surface ruptures, two conditions must be fulfilled. First, the overall surface rupture must be long enough to allow examination of a succession of several segments without being biased by segments located at the ends of the rupture. The end segments have possibly achieved only partial rupture and are not necessarily representative of the general behavior of fault segmentation during an earthquake rupture. Second, maps are needed that are accurate enough to allow identification of details of the surface rupture at a scale that is smaller than a couple of kilometers. Ideally, this should be complemented by good knowledge of the surface slip distribution. Such small scale maps are mandatory to be able to understand the details of the rupture geometry. Since earthquakes started to be documented, those two conditions have been met by only a small number of events. Analysis of the surface rupture is carried out for ten major continental earthquakes that constitute a consistent data set of rupture maps (Table 1). Although many other strike-slip earthquakes have been documented during the past century, no sufficiently detailed rupture maps are available, or the rupture was too short or partially masked by water or glaciers. Consequently, precise data for these ruptures does not exist and they had to be discarded. The 1906 San Francisco earthquake and the more recent 2002 Mw7.8 Denali earthquake are typical examples of such problematic ruptures. In the case of the 1906 earthquake, although it was probably the first time an earthquake was studied in such great detail [*Lawson et al.*, 1908], no one mapped the entire rupture in detail, and typical maps of the 1906 rupture depict a smooth and continuous surface rupture [e.g., *Segall and Lisowski*, 1990; *Thatcher et al.*, 1997]. Limited stretches of the 1906 rupture, however, have been mapped in detail (Figure 1) and these maps show that the rupture was more complex [*Scholz*, 1985], with relay zones and bends, similar to what we see for more recent, well-documented ruptures. In the case of the Denali earthquake, although a large scientific team was involved in mapping the rupture, glaciers, remoteness, and length of the rupture resulted in detailed mapping for only few areas [*Haeussler et al.*, 2004]. Hence, along these sections, the rupture geometry appears to have been complex, whereas rupture is inferred to be smoother along other sections mapped in lesser details (Figure 2).

[5] Figure 3 depicts typical geometric discontinuities that are commonly observed along strike-slip ruptures. They are of two types: fault azimuth change, or bend, and relay zones, which are also referred to as jogs. Often the two types of segment boundaries coexist. Changes in azimuth, or bends, when not associated with jogs, can be subtle and often do not exceed a few degrees. However, they have proven to be a robust criterion to distinguish discrete segments [*Bilham and Williams*, 1985] as they can significantly affect rupture propagation and earthquake time series [*Nielsen and Knopoff*, 1998; *Duan and Oglesby*, 2005]. Defining a change in azimuth may be difficult, especially if the rupture appears to be sinuous or discontinuous at a small scale. Change in azimuth does not need to be large to produce significant effects; *King et al.* [2005] have shown that a 2°

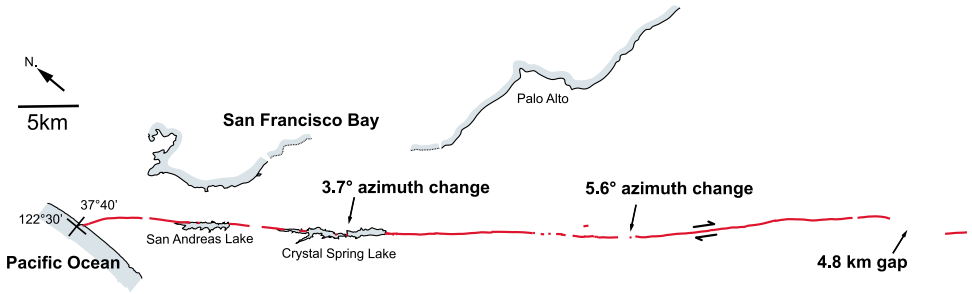

Figure 1. Surface rupture map of the 1906 earthquake south of Colma, redrawn from original maps by J. C. Branner, head of the Geology and Mining Department at Stanford University at the time of the earthquake (original notes available at the Seismological Laboratory, University of California, Berkeley). This ~75 km long stretch of rupture shows geometric complexities that are very similar to more recent, and better mapped, events of similar magnitude. The rupture makes two significant azimuth changes, and a large gap in the surface break is visible, leading to tentatively define three distinctive segments for this section of the rupture. The bend in the fault closest to the shore may also be considered, although the lack of fault visibility to the north hampers the proper evaluation of the significance of bends over longer distances.

to 3° variation in fault trace azimuth along the 2001 Kokoxili earthquake, China, was enough to promote significant vertical displacement in addition to the primarily strike-slip motion. Hence, the importance of fault-azimuth changes should not be underestimated. In the case of step over, depending on the sense the fault steps relative to the sense of fault motion, extensional or contractional features are visible. These step overs, hundreds of meters to a few kilometers wide, are, however, not always major step overs in the sense that they do not necessarily stop a dynamic rupture [*Sibson*, 1985; *King*, 1986; *Harris et al.*, 1991; *Wesnousky*, 2006].

[6] Evidence of extreme localization of faults at depth [*Chester and Chester*, 1998; *Heermance et al.*, 2003; *Sibson*, 2003; *Wibberley and Shimamoto*, 2003], along with images of the seismic source at depth [*Li et al.*, 1994; *Wald and Heaton*, 1994; *Cotton and Campillo*, 1995; *Graymer et al.*, 2007], indicate that the geometric fault complexities at the ground surface probably correspond to jumps and bends of the fault at depth. The size of associated basins, or pressure ridges, formed at segment boundaries, indicates that these features are long-lived and cannot result from a single event, but accumulate deformation from many earthquakes [*Klinger et al.*, 2006].

2.2. Automatic Segmentation Procedure

[7] One can try to agree on a simple set of rules to define segment boundaries, depending on the presence of bends or jogs along earthquake surface ruptures. Nature, however, is complex and the analyst will always bring a component of subjectivity in the interpretation of the rupture map. Hence, manual segmentation for a specific earthquake rupture will likely remain arguable. Here, I developed an automatic procedure based on a l_1 trend filtering method [*Kim et al.*, 2009] to determine the minimum number of segments needed to approximate the earthquake surface rupture, assuming that the rupture can be modeled as a series of linear segments.

[8] For each earthquake, the original rupture map is digitized. Data are re-sampled to 1pt/100m in order to ensure consistent spatial sampling of the different rupture maps, independent of the total length of each rupture. In addition, high re-sampling smoothes the data and it guarantees that the data are not affected by biased digitization due to local wiggles of the rupture trace that would have drawn involuntary attention of the operator. Similarly, high re-sampling makes the fitting procedure rather insensitive to small variations of the mapping, in the unlikely case where several maps would be available for the same rupture. In the case where the maps would be significantly different, one should still expect different results.

[9] Next, for each data set, a piecewise linear fit is achieved by minimizing the following equation:

$$\left(\frac{1}{2}\right)\sum_{t=1}^{n}(y_t - x_t)^2 + \lambda\sum_{t=2}^{n-1}|x_{t-1} - 2x_t + x_{t+1}| \qquad (1)$$

where y represents the data, x represents the model and n the number of points. Notation $|x|$ indicates the norm l_1 of vector x. In this case, the use of norm l_1 in equation (1) ensures the piecewise linearity of the fit [*Kim et al.*, 2009]. The parameter λ controls the trade-off between smoothness of x and size of RMS-misfit between the data and model, and therefore λ is a direct proxy for the number of linear segments involved in the modeling of the data. On one hand, when $\lambda \rightarrow 0$, x converges to y with a maximum number of $(n - 1)$ segments. On the other hand, it can be shown that λ_{max} exists where x converges to the best affine fit, i.e., a single segment fitting the entire data set [*Kim et al.*, 2009]. Knickpoints bounding segments result from minimization of (1) and are not determined *a-priori*. Minimization of (1) and determination of λ_{max} for each data set is performed using a MATLAB-based solver (K. Koh et al., l1_tf: Software for l1 trend filtering, 2008, available at http://www.stanford.edu/~boyd/l1_tf/) implementing a specialized primal-dual interior-point method [*Boyd and Vandenberghe*, 2004]. Figure 4 shows an example with a synthetic surface rupture map including a jog and several bends. Different fits, involving different numbers of segments, are reached depending on the value of λ.

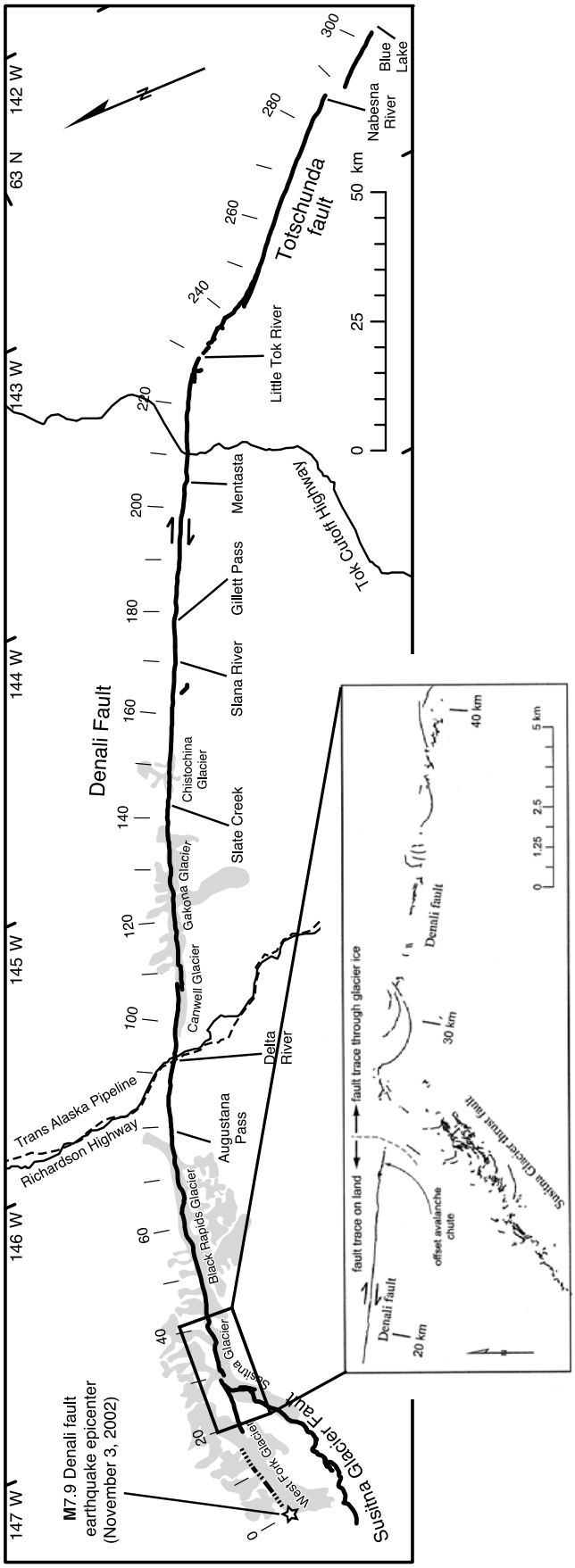

Figure 2. Surface rupture map for the 2002 Denali earthquake, Alaska, modified from *Haeussler et al.* [2004]. Most of the rupture is shown to be smooth with only few step overs and bends. In contrast, where detailed field mapping has been conducted (inset map), the rupture appears to be complex. Sections covered by ice depict a very discontinuous rupture.

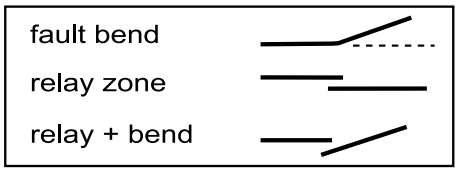

Figure 3. Typical geometric complexities observed along strike-slip faults: fault bend, relay zone (compressive or extensive), or both.

2.3. Detailed Description of Rupture Map Data Set

[10] In the following sections, rupture maps of ten earthquakes (Table 1) are analyzed in detail using the l_1 trend filtering method described in the above section, to derive fault segmentation geometries. Earthquakes have been ordered chronologically. Detailed description of the tectonic context for each event is beyond the scope of this study. For each event, basic facts about the earthquake are provided, as well as the total geological offset for the associated fault, when available. For further details, one should refer to the references listed for each earthquake.

[11] For each specific earthquake, once the surface rupture map has been digitized and the data set re-sampled, λ_{max} is computed. Then, equation (1) is minimized for a set of $\lambda \in [0, \lambda_{max}]$ and the RMS-misfit is calculated. For each event, Figure 5 shows the evolution of the RMS-misfit as a function of the number of segments involved in the fit. As predicted by the theory, when λ tends toward 0, the RMS-misfit tends to 0 for a solution with $(n - 1)$ segments, n being the total number of data-points needed to describe the surface rupture. When λ increases toward λ_{max}, the RMS-misfit increases as the number of segments involved in the fit decreases. Although the actual value of the RMS-misfit is meaningless, as it is specific to each event, the evolution of the RMS-misfit trend is significant; for all events, the RMS-misfit increases smoothly until λ reaches a threshold and then the RMS-misfit becomes subvertical to vertical, indicating that the system has reached some limit where the number of segments used to described the data becomes too small. For each earthquake, the threshold points to the minimum number of segments needed to describe the surface rupture data. The steps and changes in gradient visible for smaller values of λ correspond to segmentation at a smaller scale and are not pertinent to this study. Because the number of segments is necessarily an integer, small variations of λ can lead to the same number of segments. A slight difference in location of knickpoints, however, resulting from the trade-off between the two members of equation (1), respectively the goodness and the smoothness of the fit, can make the RMS-misfit change dramatically.

[12] For each earthquake, Figure 5 also shows one possible realization of the segmentation, which corresponds to the automatic determination of the number of segments. The specific segmentation shown for each event in Figure 5 is not unique however, and possible variations in the number and location of segment boundaries are actually discussed for each segment of each event, in view of the results from the automatic fit. Hence, possible alternative interpretations are proposed, which reflect the uncertainty estimate in the total number of required segments.

2.3.1. The 1872 Owens Valley, United States, Earthquake

[13] The Owens Valley earthquake, Mw7.5–7.7, ruptured the Owens Valley fault in 1872, producing right-lateral slip. The surface rupture (Figure 5a) of about 100 km long was not mapped in detail at the time of the earthquake. The current map is based on field notes from the time of the earthquake, complemented by more recent geomorphological studies. No detailed slip profile along the fault trace is available, although maximum horizontal slip of 10 m has been proposed [*Beanland and Clark*, 1994].

[14] Evolution of the RMS-misfit shows almost vertical increase when the number of segments is less than 5 ± 2 segments. A possible realization of this segmentation is presented in Figure 5a. Boundaries between S1 and S2 and between S3 and S4 correspond to steps of the surface trace through extensional jogs. The boundary between S2 and S3 is marked by a smaller extensional jog and a change in azimuth of the rupture trace. The boundary between S4 and S5 is more arguable, although it corresponds to a jog. Figure 4 (top) shows a simplified version of the fault map, which highlights visible changes in the fault trace azimuth.

[15] The total horizontal offset along the Owens Valley is not well established. Based on offsets of swarms of dikes and of Cretaceous plutons, it is believed to be on the order of few kilometers and does not exceed 10 to 20 km [*Beanland and Clark*, 1994].

2.3.2. The 1920 Haiyuan, China, Earthquake

[16] The 1920 Ms8 Haiyuan earthquake produced a left-laterally surface rupture along about 260 km of the Haiyuan fault. Chinese scientists have surveyed the surface ruptures and measured coseismic slip, where possible [*Zhang et al.*, 1987; *Institute of Geology*, 1990]. Because measurements were not carried out immediately after the earthquake, one should remain cautious about any interpretation of slip measurements. The fault trace at the ground surface is segmented and boundaries are mostly unambiguous (Figure 5b). The RMS-misfit increases abruptly when the surface rupture is modeled with less than 12 ± 2 segments.

[17] A possible segmentation is presented in Figure 5b and described hereafter, including some discussions about more uncertain segment boundaries. Boundaries between segments S1 and S2, S2 and S3, S3 and S4, S6 and S7 and S9 and S10 are characterized by azimuth changes of a few degrees. Boundaries between S4 and S5, S7 and S8 and S10 and S11 are marked by jogs, either extensional or contractional. At a few places, however, the interpretation is not unique: S3 has been considered a single segment based on the continuity of the rupture azimuth, which shows a sharp change both at the junction with S2 and S4. Midway along S3, however, a complicated structure corresponding to an ancient pull-apart basin is visible, which is crosscut by the 1920 rupture. Arguably, it could be considered as a segment boundary. Similarly, based on projection of the fault trace azimuth, the boundary between S5 and S6 is located in the middle of an ancient extensional basin, which does not seem to have been activated during the 1920 earthquake. Alternative segmentation models (indicated by the dashed lines in Figure 5b), where the fault trace in the basin constitutes an individual segment, is also considered, and could add one segment to the total number of segments for this rupture. Finally, the boundary between S8 and S9 is tenuous. Due to

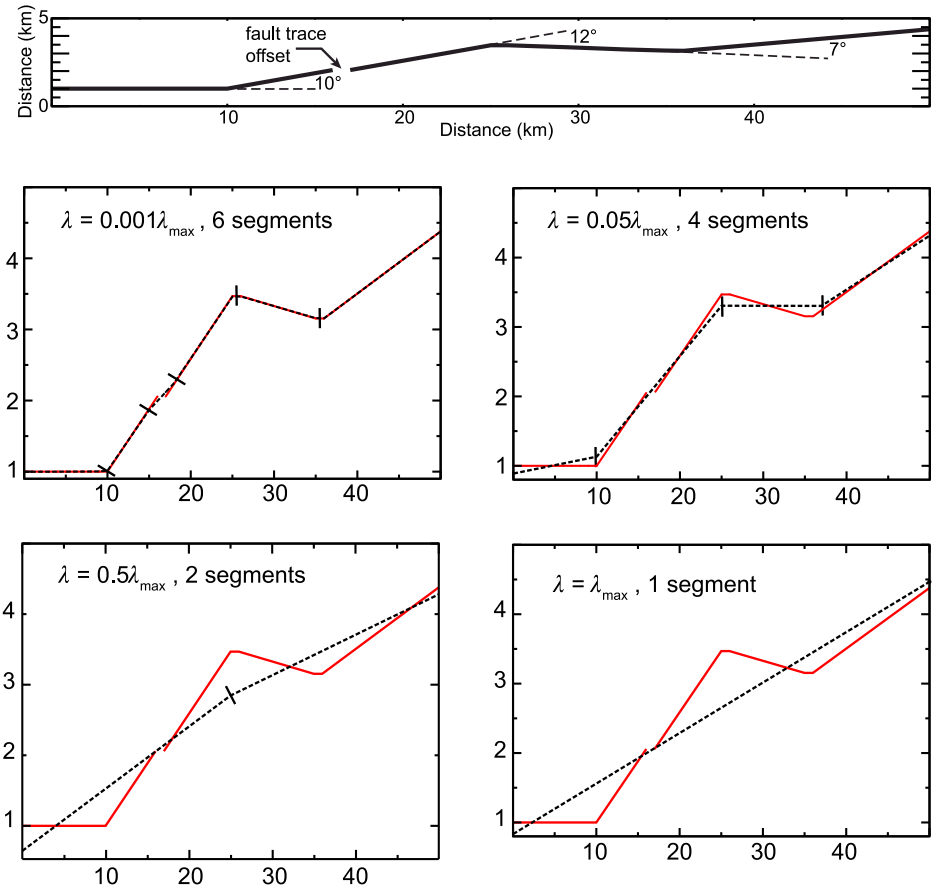

Figure 4. Synthetic example of l_1 trend filtering. (top) A typical surface rupture map, including gap/offsets and bends. One should note that the identical scales the in X and Y directions tend to visually minimize the impact of discontinuities in the Y direction. (bottom) Different models (dashed line) of the data (red line), depending on the value of λ, which controls the smoothing for a piecewise linear fit model. The scale in the Y direction has been exaggerated 10 times for better visualization. The location of kinks bounding segments (short black line) is a direct output from the minimization of equation (1).

a fault orientation that is oblique to the general direction of slip, this part of the rupture displays a significant component of thrusting, which makes interpretation of segmentation more difficult. When observed in detail, however, a small misalignment is visible that produces a compressive jog along this part of the rupture, which could be interpreted as a segment boundary.

[18] The total displacement for the Haiyuan fault is not well defined but based on lateral offset of geologic units and of the Yellow river streambed, it is assumed to be of the order of 125 km [*Replumaz and Tapponnier*, 2003].

2.3.3. The 1957 Gobi-Altay, Mongolia, Earthquake

[19] The 1957, Ms8.3 Gobi-Altay earthquake broke about 240 km of the left-lateral Bogh fault. It is one of the largest continental earthquakes of the last century, although the total horizontal displacement does not exceed ~25 km [*Kurushin et al.*, 1997].

[20] The geometry of the surface rupture trace (Figure 5c) for this event is more complex than rupture for other events considered in this study, primarily because the strike-slip was accompanied by a significant component of thrusting at many locations along the fault [*Florensov and Solonenko*,

Figure 5. For each event in our earthquake data set, we present the l_1 trend filtering analyses along with the original surface rupture trace. The break in slope in the RMS-misfit trend is indicated. The uncertainty depends on the sharpness of the bend in the RMS trend. Despite the fact that models for a very large number of segments are always calculated, they are not always represented because of some de-noising procedure in our implementation of the l_1 trend filter. Nevertheless, this part of the RMS-misfit trend is trailing smoothly toward 0 with an increasing number of segments and thus can be ignored. For each event, a possible segmentation is presented, which is in agreement with the independent result of the l_1 trend filtering. Note that the same scales in both the X and Y directions tend to visually minimize the disruption of the fault trace in the Y direction, especially when the rupture trace is long. Black lines indicate segment limits. When several interpretations are possible (see text), vertical dash lines show alternative possibilities. As discussed in the text, in the case of the 2001 Kokoxili earthquake, the detailed surface trace is not available along the entire rupture. This is accounted for by evenly distributed and unusually dense horizontal coseismic slip measurements along the strike-slip section of the rupture.


schematic represention of S1, S2 and S3
N.
S1
S2
S3
S4
S5
7° azimuth change
5° azimuth change
10km
Ⓐ 1872, Owens Valley earthquake
N.
S1
S2
S3
S4
S5
S6
S7
S8
S9
S10
S11
Azimuth change 14°
Azimuth change 15°
Azimuth change 3°
Azimuth change 14°
10 km
Ⓑ 1920, Haiyuan earthquake
99°00E
99°30E
100°00E
100°30E
101°00E
101°30E
102°00E
45°00N
N.
S1
S2
S3
S4
S5
S6
S7
S8
S9
S10
S11
S12
S13
S14
S15
4° azimuth change
16° azimuth change
10° azimuth change
10km
Ⓒ 1957, Gobi-Altay surface ruptures
5 ± 2 segments
RMS misfit
nb of segments
12 ± 2 segments
RMS misfit
nb of segments
14 ± 2 segments
RMS misfit
nb of segments

Figure 5

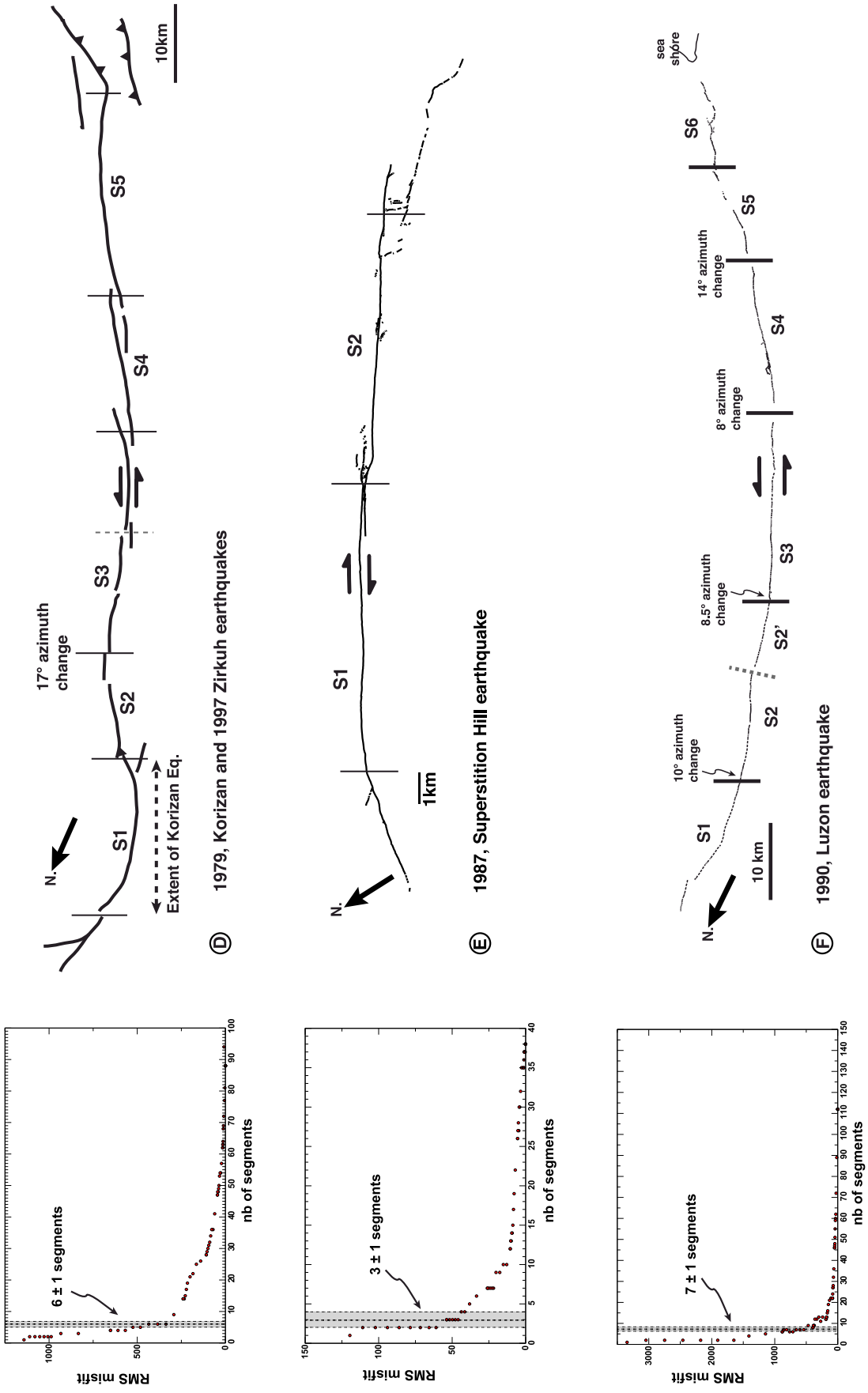

Figure 5. (continued)

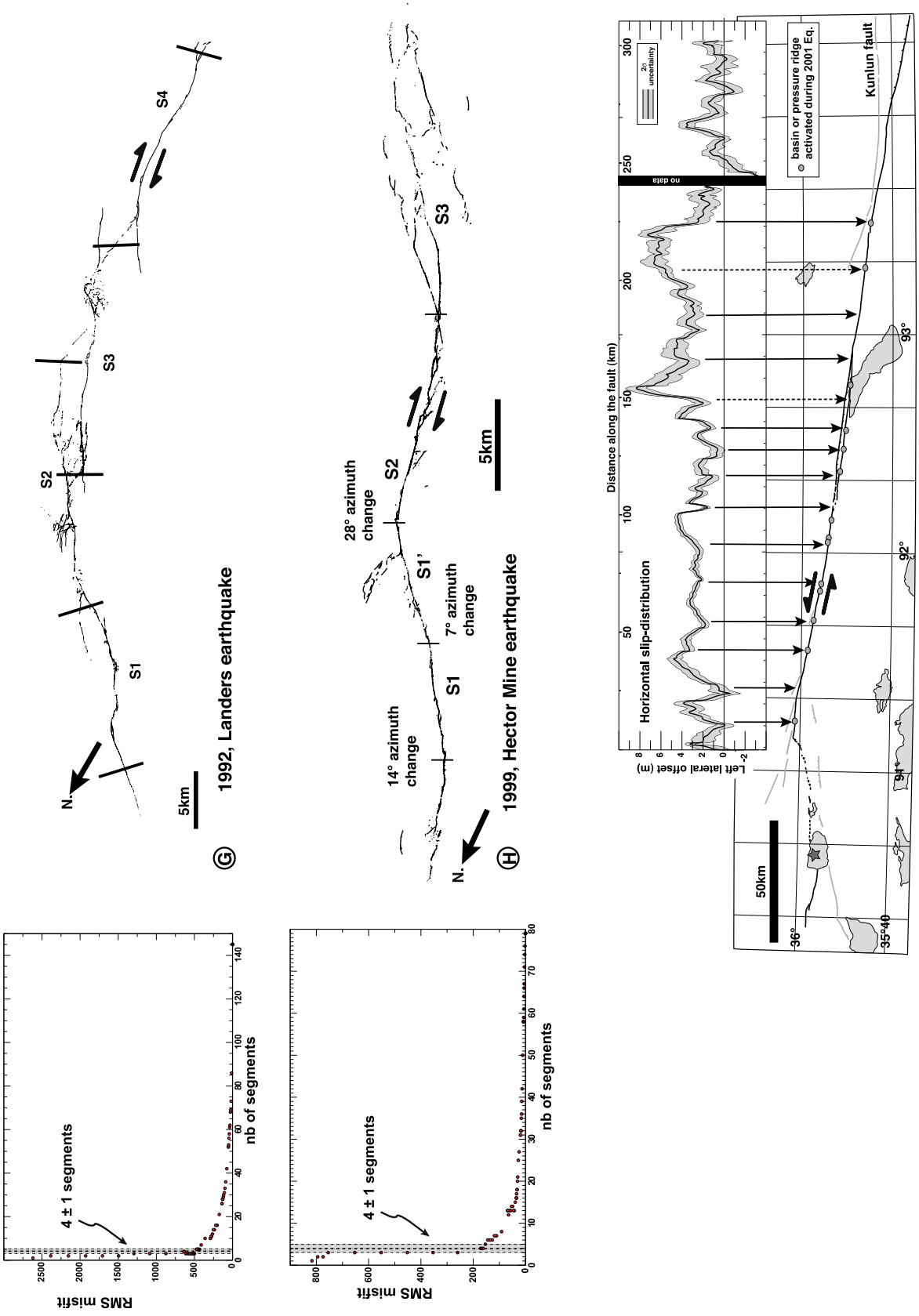

Figure 5. (continued)

1965; *Kurushin et al.*, 1997]. Segment boundaries, however, mostly based on changes in azimuth of rupture and on relay zones, are clearly expressed in the morphology. The RMS-misfit unambiguously rises almost vertically when one tries to model the surface rupture using less than 14 ± 2 segments.

[21] A possible segmentation model is presented in Figure 5c. The number of segments is rather well established, although the exact location of the boundaries can easily be shifted laterally due to numerous large overlap areas. Azimuth changes of few degrees characterize the boundaries between S1 and S2, S4 and S5 and S5 and S6 (see below about S6). A boundary may also exist between S10 and S11, which would be associated with an azimuth change of 10° and with perpendicular intersection of the main rupture with a secondary fault. Boundaries between S2 and S3, S3 and S4, S8 and S9, S9 and S10, S11 and S12, S12 and S13, S13 and S14 and S14 and S15 are all characterized by jogs, most of which are extensional. Interpretation of segmentation at the boundary between S6 and S7 is problematic. At this location, the rupture trace steps northward along S7, which accommodates almost pure thrusting. The strike-slip motion seems to be concealed and S6 is acting like a lateral ramp. Hence, interpretations in which S6 and S7 constitute one or two segments are both possible.

2.3.4. The 1979 Korizan, Iran, Earthquake

[22] The Mw6.6 right-lateral Korizan earthquake ruptured part of the Abiz fault in 1979 [*Berberian et al.*, 1999]. This event broke segment S1 of the Zirkuh earthquake (Figure 5d, see section 2.3.8 about the Zirkuh earthquake) but did not extend farther along the Abiz fault. Because only one segment broke, l_1 trend filtering is meaningless and it has not been used here. Due to the small magnitude, deformation at the surface is small and coseismic slip is ≤1m. However, the lateral extent of the rupture is well documented by field reports [*Berberian et al.*, 1999] and this rupture can be used for further analyses. See the Zirkuh earthquake, in section 2.3.8, for discussion about the total offset along the Abiz fault.

2.3.5. The 1987 Superstition Hills, United States, Earthquake

[23] The M6.6 right-lateral Superstition Hills earthquake ruptured the southern part of the San Jacinto fault system in 1987 [*Sharp et al.*, 1989]. Total length of the surface rupture was about 26 km. The southern part of the rupture, however, does not carry significant slip and it has not been included in the analysis. The rupture is clearly divided in two segments S1 and S2, separated by a narrow dextral step over (Figure 5e). The slip distribution from field measurements defines the same two distinct patches of slip [*Sharp et al.*, 1989]. Interestingly, after-slip along the Superstition Hills was larger than usually observed for earthquakes, and it was also distributed along the same two segments. Application of l_1 trend filtering in this case is not very useful due to the obvious character of segmentation and the small number of segments. Filtering, however, shows a drastic rise of the RMS-misfit for a number of segments less than 3 ± 1. The third segment corresponds to the small continuation of the rupture, next to S2, across the jog. This case demonstrates the robustness of the filtering methods even for a small number of segments.

[24] Total offset along the Superstition Hills fault is not well documented. The best estimate is the ~20 km total strike-slip documented for the San Jacinto fault system, which the Superstition Hills fault is part of [*Sharp*, 1967].

2.3.6. The 1990 Luzon, Philippines, Earthquake

[25] The 1990, Mw7.8, left-lateral Luzon earthquake is one of the largest instrumental strike-slip earthquakes that has been recorded. It ruptured at least 120 km of the left-lateral Philippine fault. The total rupture length, however, is not known as the rupture propagated southward and ended offshore of Luzon Island [*Yoshida and Abe*, 1992]. Although high levels of rainfall under tropical conditions result in poor preservation of the coseismic deformations, observations collected shortly after the event allow for a good ground surface rupture map (Figure 5f), together with slip measurements [*Nakata et al.*, 1996].

[26] Application of l_1 trend filtering to the Luzon rupture shows an abrupt rise of the RMS-misfit for models including less than 7 ± 1 segments. Figure 5f shows a possible segmentation of the surface rupture, including alternative possibilities for segments S2 and S2′. Overall, the Luzon rupture is mostly characterized by large azimuth changes (8° or more), often co-located with ground rupture trace disruptions. Hence, segment boundaries between S1 and S2, S2′ and S3, S3 and S4 and S4 and S5 are all based on azimuth changes. Both S5 and S6 have been considered individual segments based on the uniformity of the trace azimuth along these sections, despite short ground rupture trace disruption or side branches. The boundary between S5 and S6 corresponds to a contractional jog, associated with a change in azimuth. The boundary between S2 and S2′ is poorly defined. Over a distance of a few kilometers, the fault trace seems to change azimuth and to move westward, justifying the choice of a segment boundary. However, at the scale of 10 km to 15 km, the azimuths of S2 and S2′ are similar and they could be considered as one segment.

[27] Total offset along the Philippine fault is not well known. Based on strike-slip offsets of geological markers, values vary from 100 to 200 km since the Miocene [*Karig*, 1983; *Mitchell et al.*, 1986; *Pinet and Stephan*, 1990].

2.3.7. The 1992 Landers, United States, Earthquake

[28] The Mw7.3 Landers earthquake ruptured several right-lateral faults in southern California (Figure 5g). The surface ruptures and distribution of slip was documented over a distance of ~80 km [*Sieh et al.*, 1993; *Arrowsmith and Rhodes*, 1994; *Johnson et al.*, 1994; *Sowers et al.*, 1994; *Zachariasen and Sieh*, 1995; *McGill and Rubin*, 1999]. The faults that ruptured in the Landers earthquake comprise en-echelon segments separated by relay zones. Processing of the data set with l_1 trend filtering shows that the RMS-misfit starts to rise vertically when the surface rupture is modeled with less than 4 ± 1 segments. As in the case of the Goby Altai rupture, the segmentation of the Landers rupture is well established, based on preeminent extensional basins. The exact location of segment extremities, however, is arguable depending on where one places the boundaries inside basins. To the northeast, the overlap between the Camp Rock segment, S1, to the North and the Emerson segment, S2, is long (~10 km) and both segments carry significant slip in the overlap zone [*Sieh et al.*, 1993]. Although the overlap between segments S2 and S3 is ~10 km long, most of the slip in the overlap occurred on S3 [*Sieh et al.*, 1993; *McGill and Rubin*, 1999]. Hence, the boundary between S2 and S3 was located at the northeast

end of the step over. The overlap between S3 and S4 is shorter than the two steps described before. The slip on the southern end of S3 and the northern end of S4 decreases rapidly, with most of the slip being transferred through a trans-tensional structure [*Spotila and Sieh*, 1995]. Hence, we arbitrarily put the boundary between S3 and S4 midway between the southern end-point of S3 and the northern end-point of S4.

[29] The total offset across the East California Shear zone, including the Landers rupture, is larger than 40 km, although offset on individual faults might be as small as few kilometers [*Jachens et al.*, 2002].

2.3.8. The 1997 Zirkuh, Iran, Earthquake

[30] The 1997, Mw7.2 Zirkuh earthquake ruptured the northern part of the Abiz fault (Figure 5d). The Abiz fault is one of the main structures bounding the Luth block to the East. Total offset along this fault has been estimated to be ~80 km [*Walker et al.*, 2004].

[31] The total length of the 1997 rupture is 175 km. Here, however, analysis is confined to ~100 km of the rupture that correspond to the main strike-slip section; other parts of the rupture, mostly to the south, display almost pure thrusting [*Berberian et al.*, 1999]. Unlike other earthquakes considered here, the surface rupture fault map is not available in great detail. Only a kilometric-scale map is available. On the other hand, slip distribution, complemented by field descriptions, is rather well documented [*Berberian et al.*, 1999]. Despite the relatively low quality of the ground rupture documentation, the l_1 trend filtering of the data shows that the RMS-misfit rises unambiguously when the number of segments is less than 6 ± 1.

[32] A possible segmentation, in agreement with the results from the automatic filtering, is described hereafter (Figure 5d), based on the ground ruptures and, when necessary on the surface slip distribution [*Berberian et al.*, 1999]. A contractional jog and a sharp drop in coseismic slip to zero mark the boundary between S1 and S2. The location of this boundary could arguably be slightly shifted northward to better fit the location of the fault trace azimuth change and a fault intersection point. This, however, would not significantly impact the segmentation model of the ground rupture trace. To the north, the S1 termination has been located where the coseismic slip reaches zero, at a relay zone. It is worth noting that segment S1 also ruptured by itself in the 1979 Korizan earthquake, showing that segments persist over multiple earthquakes [*Sieh*, 1996]. The boundary between S2 and S3 is marked by a 17° azimuth change in the surface rupture trace. The boundary between S3 and S4 is marked by an extensional relay zone and a drop in the coseismic slip. Arguably, S3 could be subdivided into two shorter segments, midway along the segment, as a secondary rupture runs parallel to the main trace. However, according to the slip distribution, this secondary rupture does not seem to significantly affect the rupture process on the main fault. In addition, the azimuth of the main rupture remains unchanged south of this debatable boundary. The boundary between S4 and S5 also corresponds to an extensional jog in the surface rupture trace, and a drop in coseismic slip. Although S5 seems to extend northward of the boundary location, field notes and slip measurements indicate that S5 actually accommodated only minor slip (~20 cm) along its northern extension and that most of the slip (~70 cm) is immediately transferred on S4 during the 1997 earthquake.

2.3.9. The 1999 Hector Mine, United States, Earthquake

[33] The Mw7.1 Hector Mine event ruptured right-lateral faults of the Mojave Desert. The ground rupture has been carefully mapped in the field (Figure 5h) and wherever possible, coseismic slip was measured [*Agnew et al.*, 2002; *Hudnut et al.*, 2002; *Simons et al.*, 2002; *Treiman et al.*, 2002]. The total length of the rupture is about 48 km, including several parallel strands in the south that did not sustain lateral displacement but only ground surface cracking. The epicenter was located along a ~5 km long side segment that connects to the main rupture zone. Total geological offset is not well established as the slip rate is small and geologic piercing points are rare. Based on magnetic anomaly pairs, total geologic offset along the faults that broke during the Hector Mine earthquake does not exceed 10 km [*Jachens et al.*, 2002].

[34] The l_1 trend filtering is straightforward in the case of Hector Mine and the RMS-misfit shows a sharp increase for models with less than 4 ± 1 segments. A possible segmentation is shown in Figure 5h, mainly constrained by sharp azimuth changes (≥7°). Because some azimuth changes are very large along the Hector Mine rupture, segments S1 and S2 might be considered as a single segment as the change in azimuth is only 7°, which is small compared to other azimuth changes. To remain consistent with rules about azimuth change applied to other ground rupture maps analyzed here, we favor a two-segment interpretation. North of S1, the rupture can be followed for a few more kilometers before it dies out, not carrying any significant slip. To the south, the ground ruptures divide into three parallel strands of similar length. Only one accrued measurable slip in 1999, the two others exhibited ground cracking only. Here, we only consider the segment that accommodated significant slip, as the tectonic significance of the two other segments remains unclear.

2.3.10. The 2001 Kokoxili, China, Earthquake

[35] The Mw7.8 Kokoxili earthquake ruptured the Kunlun fault for about 430 km (Figure 5i). The Kunlun fault is one of faults bounding the Tibetan plateau to the North. Total left-lateral offset along this fault has been estimated to be ~150 km [*Van Der Woerd et al.*, 2002]. Extreme remoteness, high altitude (≥4000m) and the unusual length of the coseismic rupture (430 km) have prevented the 2001 ground rupture from being mapped in its totality in the field, precluding the use of l_1 trend filtering.

[36] Nevertheless, a few long sections of the rupture have been mapped using high-resolution satellite images and have been checked in the field at key locations [*Klinger et al.*, 2005; *Li et al.*, 2005; *Xu et al.*, 2006]. In addition, high-density slip distribution has been derived from correlation of pre- and post-earthquake optical satellite images, and cross-checked against field data [*Klinger et al.*, 2006]. This method has allowed us to determine an along-strike slip-profile with one horizontal slip measurement per kilometer, evenly distributed along the strike-slip section of the rupture (~300 km). The western and eastern ends have been discarded as they accommodate a significant component of vertical motion [*Xu et al.*, 2002; *Klinger et al.*, 2005].

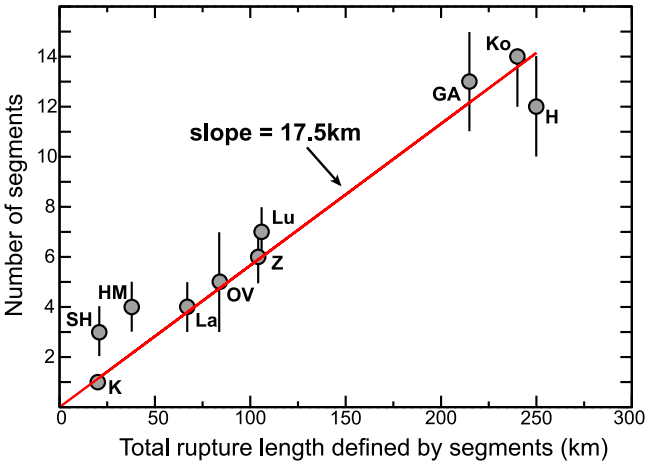

Figure 6. Best fit linear regression between the number of segments computed from the l_1 trend filtering for each earthquake and the total length of a rupture that is considered to define these segments. The inverse of the slope of the best fit line gives the average length of segment for the data set. K: Korizan, SH: Superstition Hills, HM: Hector Mine, La: Landers, OV: Owen Valley, Z: Zirkuh, Lu: Luzon, Ko: Kokoxili, GA: Gobi Altay, H: Haiyuan.

[37] The Kokoxili rupture changes azimuth only three times along the strike-slip section. This occurs at the beginning and end of the section where slip-partitioning between strike-slip and normal motion is observed (Figure 5i, km 100 to km 175) [*King et al.*, 2005] and, also where the rupture propagated southward (Figure 5i, km 230), away from the main continuation of the Kunlun fault. Azimuth changes are ~3° and ~6°, respectively. Instead of multiple changes of azimuth, the Kokoxili rupture is characterized by numerous steps that range from a few hundred meters to a kilometer in size; these create compressional and extensional jogs. The along-strike slip-distribution reflects these perturbations of fault geometry, as each geometric complexity is characterized by low values in the slip-distribution curve. Following *Klinger et al.*, [2006], we use the conjunction of geometric complexities visible in the field and on satellite images (all reported on ground rupture map) and the slip-distribution to break the Kokoxili rupture into 14 +0/−2 segments along the strike-slip part of the rupture.

2.4. Segment Length Summary

[38] For each of the ten earthquakes analyzed in Table 1, Figure 6 shows the number of segments defined for each event using the l_1 trend filtering method versus the total length of the surface rupture considered to define segments. The Korizan and Kokoxili earthquakes have also been included. Circles indicate the number of segments determined by the analyses of the RMS-misfit trend, along with their associated uncertainties. Taking the inverse of the slope for the best linear fit gives the average segment length for the entire data set. In this case, the average length segment is 17.5 km with a coefficient of correlation of 0.98 for the best linear fit. This average segment length is not affected significantly by uncertainty in the number of segments considered for each earthquake. Because one can compute a linear fit with a high coefficient of correlation, this suggests that the average segment length is independent of the tectonic setting of individual earthquakes and should be linked to intrinsic physical properties of the brittle crust. The simplest geometric relations suggest that it should be the thickness of the seismogenic crust.

[39] If the thickness of the continental crust, with a lower boundary defined by the Moho, varies significantly depending on the geological context, it appears that variations of the seismogenic crustal thickness tend to be much smaller. The continental crust in California and in the Philippines is estimated to be between 30 and 35 km in thickness [*Mooney et al.*, 1998]. In China, Mongolia and Iran, the continental crust is believed to be thicker, between 40 and 45 km [*Mooney et al.*, 1998]. The thickness of the seismogenic crust, with a lower limit that can be defined by the extent of seismicity at depth [*Scholz*, 1990], shows smaller variations, at least in the continental domain. On the Tibetan plateau, the maximum depth for earthquakes has been documented to be about 20 km [*Chen and Molnar*, 1983; *Molnar and Chen*, 1983; *Lasserre et al.*, 2001; *Yang et al.*, 2005; *Chu et al.*, 2009]. In Mongolia, the maximum depth of the background seismicity is also about 20 km, although a few events have been documented to be deeper [*Déverchère et al.*, 2001; *Bayasgalan et al.*, 2005]. Geodetic measurements in northern Mongolia suggest that the seismogenic crust could be as thick as 25 km [*Calais et al.*, 2003]. The seismicity in the Philippines, for the part that is not related to subduction, is also limited to 20 to 25 km [*Galgana et al.*, 2007]. Background seismicity in Iran seems to be more superficial with a lower limit for the seismicity around 15 km [*Maggi et al.*, 2000; *Engdahl et al.*, 2006]. Similar observations have been made in Southern California [*Nazareth and Hauksson*, 2004]. Thus, for all of the regions considered here, the thickness of the seismogenic crust is limited to between 15 and 20 km, which corresponds well to the 17.5 km average length of individual segments.

[40] Although very speculative due to sparseness of data, it is worth noting that a few earthquakes in California (Hector Mine and Superstition Hills, but not Landers) seem to have segments that are shorter than average. In contrast, the Haiyuan event seems to have segments that are longer than average. If, as suggested here, segmentation is linked to crustal thickness, this would be in good agreement with evidence that suggests thinner than average seismogenic crust in southern California [*Nazareth and Hauksson*, 2004] and thicker than average seismogenic crust in the Haiyuan fault area [*Lasserre et al.*, 2001].

[41] Further insights can be gained if one looks at the distribution length of individual segments for the earthquake data set. Based on the possible segmentation shown on Figure 5, which is in agreement with the l_1 trend filtering results, Figure 7 shows the length of all individual segments measured (64 in total) for each event. Although Figure 7 indicates that considerable natural variation exists in the local geometry of ground rupture traces, the average length of segments can be determined with a good level of confidence to be 17.9 km ± 5.2 km, independently of specific tectonic conditions. Interestingly, segments longer than the 1σ upper bound exist, but all segments fall within 2σ interval. Moreover, there are no very long segments found in the data set. If such long segments had been observed, it would have indicated that fault traces can be permanently smoothed out

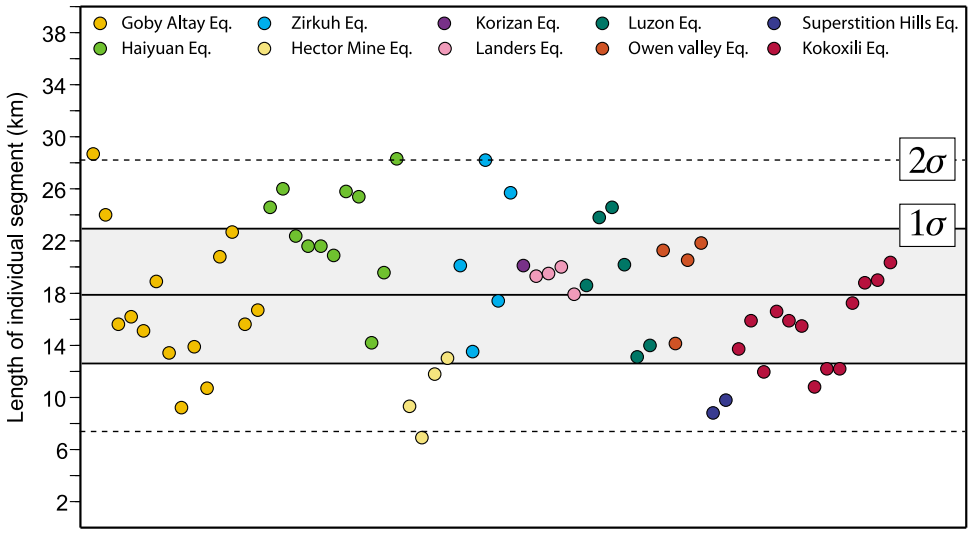

Figure 7. Plot of the length for individual segments presented in Figure 5. The mean length is 17.9 km, and the shaded area indicates the 1σ interval. The dashed lines denote the 2σ range. The range of possible values is limited, and more importantly, no very large values are observed.

over very large offset amounts (>20 km) [*Wesnousky*, 1988; *Manighetti et al.*, 2007].

3. Slip Maps Derived From Kinematic Inversion

[42] Kinematic inversions of seismic and geodetic data are routinely used to create models of static displacement on finite faults. While kinematic inversions remain among the best tools to image the earthquake source, they are problematic because quantifying the error in models is difficult [*Page et al.*, 2009]. Hence, consensus on the coseismic slip among different studies is not always achieved; the location and amplitude of slip on the fault plane can differ significantly between studies for a particular event [*Beresnev*, 2003; *Clévédé et al.*, 2004; *Zhou et al.*, 2004]. Due to the limited data set pertinent to the source determination, in practice the inverse problem is often underdetermined. This means that the available data are not sufficient to uniquely determine every source parameter [*Chen et al.*, 2002a; *Page et al.*, 2009]. Typically, kinematic inversions often suggest that seismic sources do not extend deeper than 15 km to 25 km to achieve an acceptable fit to the data, when this parameter is actually not well constrained in most inversions and is subject to large trade-offs with other source parameters [*King and Wesnousky*, 2007]. Hence, large differences in published solutions for particular earthquakes arise from differences in the data sets considered, sampling of different frequency bands and, therefore, imaging different characteristics of the seismic source. In addition, inversion schemes and weighting of data can also be quite different, producing different solutions from similar data [*Sudhaus and Jonsson*, 2009]. Despite such a pessimistic preamble, several studies have shown that preeminent features of a source model, such as size and amplitude of the main slipping area, but not necessarily location of such an area, can be robust if the earthquake is large enough and inversions are performed with care [*Beresnev*, 2003; *Vallée and Bouchon*, 2004; *Hartzell et al.*, 2007; *Page et al.*, 2009].

[43] We have selected 17 continental strike-slip earthquakes with magnitude ≥6 (Table 2), from the SRCMOD database (M. Mai, Database of finite-source rupture models, 2007). The SRCMOD database collects published finite-source rupture models that image the spatiotemporal evolution of earthquake rupture through modeling/inversion of seismic and/or geodetic data. For each earthquake, the SRCMOD database provides slip-distributions on the fault plane, derived from the different reliable seismic source solutions published in the literature, all in a standardized format. In addition to continental strike-slip events, one strike-slip event that occurred on an oceanic transform is also shown for comparison. For a complete assessment of all the strike-slip sources selected here, and for an overview of each event in its tectonic context, the reader is directed to refer to the reference list included in the SRCMOD database (M. Mai, Database of finite-source rupture models, 2007). For each earthquake in this data set, we have measured the horizontal dimension of the largest patch of slip visible on each slip-map (Figure 8). Measurement was performed by

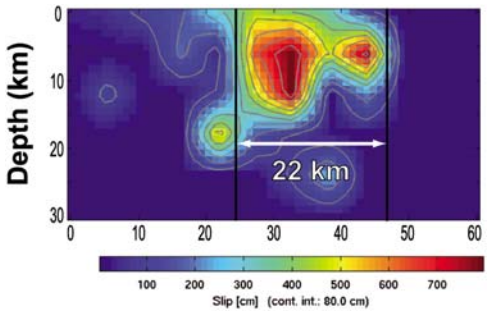

Figure 8. Kinematic inversion for the Mw 7 Duzce event (Turkey, 1999), which has only one large slip-patch [after *Delouis et al.*, 2004]. Details of the slip inversion might be beyond actual resolution of the data, but the main slip patch is well determined.

Table 2. Strike-Slip Earthquakes for Which Slip Maps Are Available That Were Used to Measure the Lateral Extent of Slip-Patches[a]

Name/Region	Date (mm/dd/yy)	Mw	Event
Gifunken Chubu (Japan)	09/09/69	6.43	1
Izu Hanto Oki (Japan)	05/09/74	6.56	2
Oitaken Chubu (Japan)	04/21/75	6.38	3
Imperial Fault (United States)	10/15/79	6.5	4
Izu Hanto Toho (Japan)	06/29/80	6.58	5
Nagano Ken Seibu (Japan)	09/14/84	6.3	6
Elmore ranch (United States)	12/24/87	6.55	7
Superstition Hills (United States)	11/24/87	6.5	8
Joshua Tree (United States)	04/24/92	6.2	9
Landers (United States)	06/28/92	7.2	10
Kobe (Japan)	01/17/95	6.9	11
Antarctica	25/03/98	7.9	12
Duzce (Turkey)	11/12/99	7.1	13
Hector Mine (United States)	10/16/99	7.2	14
Izmit (Turkey)	08/17/99	7.4	15
Tottori (Japan)	10/06/2000	6.8	16
Denali (United States)	11/14/2002	7.9	17
Kokoxili (China)	11/14/2001	7.8	18

[a]The event number refers to Figure 8. Full references for individual inversions are given by M. Mai (Database of finite-source rupture models, 2007).

semi-automatic picking of patch limits based on color-coding of slip on the slip-map. The spatial resolution of slip maps is dependent upon the kind of data inverted, data coverage, inversion scheme and magnitude of earthquake [*Page et al.*, 2009]. Thus, the data resolution issue should be kept in mind when comparing different source inversions for the same event. Here, when several inversion results were available, measurements were carried out for all solutions and we used the mean value and standard deviation as a dispersion estimate. For events with magnitudes of approximately 7 or less, slip distribution is usually limited to only one main patch of high slip (one to a few meters). Automatic picking of the edges of this patch is unambiguous at the 2m limit, which is the amount of slip that is assumed to be resolved in geophysical inversions for events of this magnitude.. For earthquakes with magnitude ≥7, high slip is generally distributed on several high-slip patches that can be distinguished visually, based on slip gradients. However, due to smoothing functions that are often introduced in the inversion processes to limit sharp lateral slip variations, the edges of slip patches tend to smear and to connect to nearby patches, making automatic picking more difficult. Decreasing or increasing the limit value that defines the edges of a patch can affect the length measurements rather differently. On one hand, if the limit is decreased (which is unreasonable due to the lack of resolution in geophysical inversions), the lengths of the patches grow larger and, due to numerical smearing, it quickly becomes impossible to distinguish between adjacent patches. On the other hand, increasing the limit value has a limited impact on the size of the patch, as the gradient of slip inside a slip-patch is generally high.

[44] Figure 9 shows length of the largest slip patch against earthquake magnitude for our data set. The lowest magnitude considered is ~6. It appears from this plot that the maximum horizontal dimension of a slip patch does not increase infinitely with magnitude, but rather seems to saturate for large magnitudes to a value close to 25 km in length. This suggests that when large earthquakes nucleate and propagate along the fault to eventually form a large rupture, propagation of the rupture is actually controlled and somehow limited by the lateral structure of the fault, which is characteristically ~25 km in size. This characteristic size is of the same order as the thickness of the seismogenic crust [*Lee et al.*, 2002]. It is not surprising, therefore, that the only strike-slip earthquake in our data set that occurred in oceanic crust (event 12 in Figure 9), the Mw7.9, 1998, Antarctica earthquake [*Antolik et al.*, 2000] does not fit the general observation. In contrast, this event appears to have a shorter horizontal dimension of slip patches, in agreement with the fact that it occurred in the thinner oceanic crust.

[45] Although it could unfortunately not be checked for all events for which surface ruptures are presented because of the lack of pertinent data and/or resolution, one can cross-check the slip distribution of the surface ruptures against kinematic inversions for two very well documented earthquakes from our data set, the 1992 Landers and 1999 Hector Mine earthquakes. In both cases, independent studies show a good agreement between the number and the location of segments determined here and the location of slip patches derived from inversion of geophysical data [*Freymueller et al.*, 1994; *Wald and Heaton*, 1994; *Chen et al.*, 2002b; *Kaverina et al.*, 2002; *Simons et al.*, 2002]. In these cases, geophysical data were processed in parallel with the collection of the field-based rupture data. Hence, the main characteristics of ruptures, as observed in the field, were acknowledged by the authors of the various geophysical studies, but were generally not incorporated as a primary source of data into their work. A different result should be expected for earthquakes involving dip-slip, such as normal fault events or subduction earthquakes, where geo-

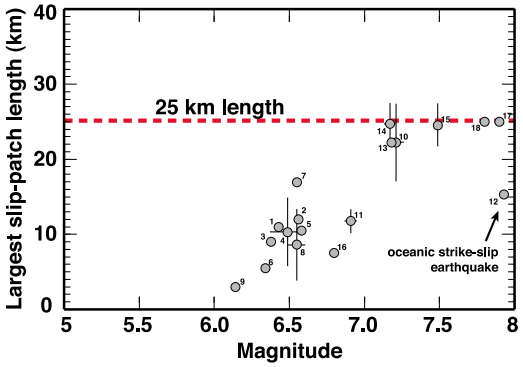

Figure 9. Maximum horizontal extent of slip-patches measured from slip inversion maps for events listed in Table 2. For earthquakes with magnitude ≤7, the seismic source is usually limited to one circular slip patch with a radius that is equal or smaller than the thickness of the seismogenic crust. For larger events, the source divides into multiple subevents, where the maximum horizontal extent saturates at about 25 km. Interestingly, the maximal horizontal extent for the oceanic strike-slip event (event 12), included for comparison, is much shorter, as expected for thinner seismogenic crust.

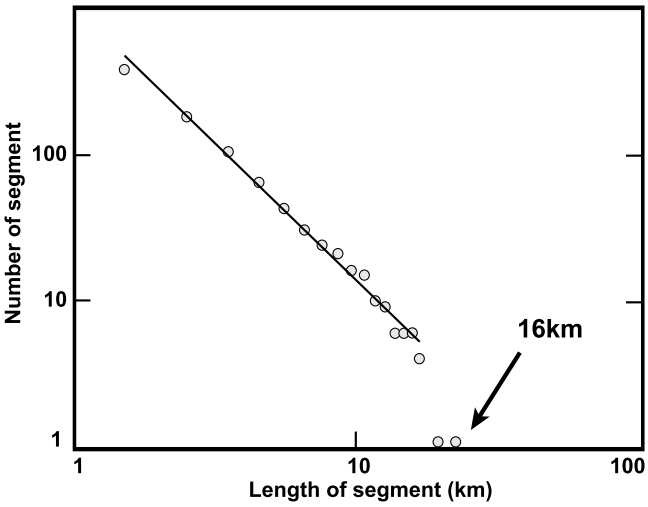

Figure 10. Number of segments with respect to their length along the San Andreas Fault, central California. The data are well described by a power law $Y = 1031.5*X^{(-1.89050)}$, R = 0.99395, which is characteristic of a fractal distribution. This distribution, however, saturates for a maximum value of ~16 km, with no larger segments. This value is in good agreement with the local crustal thickness. Data from *Wallace* [1973], redrawn from *Scholz* [1998].

metric constraints on the width of the seismic source are very different.

4. Discussion and Conclusions

[46] These two independent lines of evidence show that faults are laterally structured, i.e., segmented, and that this structure has an average characteristic size of 21 km ± 4 km. Because this value is derived from observations of earthquakes at various locations, this behavior appears to be independent of any specific geological setting. Instead, it is likely related to some basic property of the breaking medium. The average 21 km segment length is similar to the thickness of the brittle crust, which is usually estimated to be between 15 and 25 km, based on background seismicity and aftershock depth distributions (see *Lee et al.* [2002] and references for specific areas in section 2.4). Hence, we propose, based on those observations, that the length of fault segments, in the case of continental strike-slip faults, is linked to the thickness of the brittle crust.

[47] Although the 1:1 scaling between the size of the segments for a crustal fault and the thickness of the brittle crust has long been considered to be intuitively correct, it has proven to be difficult to demonstrate [*Scholz*, 1990, 1998]. The regularity of the length of fault segments had been pointed out for some sections of large strike-slip faults outside the context of individual large earthquakes: The San Andreas fault, in the Coachella Valley, locally displays a sawtooth geometry with segments that are typically about 12 km long, as defined by azimuth changes. In this region, the deepest earthquakes are located at 12 km [*Bilham and Williams*, 1985; *Wallace*, 1989]. Along the central part of the San Andreas fault, a similar segment pattern has been observed [*Wallace*, 1973; *Scholz*, 1998] with average segment lengths of about 16 km (Figure 10).

[48] The mechanical principles that result in fault segment lengths that scale proportionally with the thickness of the seismogenic crust is not yet fully understood, but some analog experiments provide support for this interpretation. Reanalysis of a strike-slip experiment by *Schlische et al.* [2002] shows that during the early stages of shearing of a clay cake, extensional cracks form oblique to the main shear direction. At some point, the extensional cracks stop increasing in length and a pure shear rupture aligns with the main direction of shearing. Careful measurements of the length of the cracks at their maximum extent indicate that on average their lengths are approximately equal to the 4 cm thickness of the clay-cake used in this specific experiment, confirming a very simple geometric relation that links the thickness of the breaking medium to the length of the segments (Figure 11).

[49] As with clay cake experiments, faults that propagate through pristine rock first create cracks that are similar to extensional cracks seen in the analog experiment [*Scholz*, 1990]. Because it should be easier to propagate through weaker rock, subsequent ruptures along the same fault system will tend to rotate blocks and re-use the path formed by those early cracks instead of creating a new shear fractures [*Armijo et al.*, 1989]. This likely occurs even though they may not be optimally oriented for shear, Thus, new fractures link the oblique cracks through what is interpreted in the field as relay zones. However, due in part to preexisting geological structures [*Mann*, 2007], these heterogeneities, must influence the path of a real fault when it

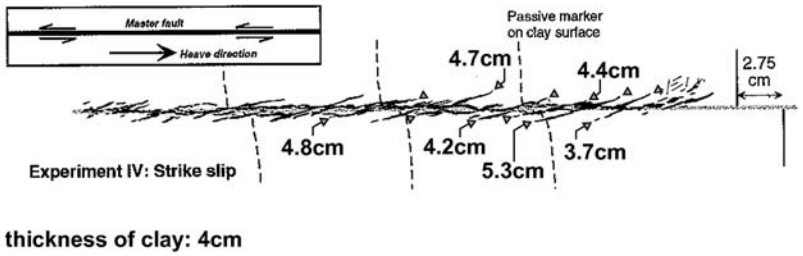

Figure 11. Strike-slip experiment in clay after *Schlische et al.* [2002]. Triangles point to extremities of oblique fractures (similar to R1 Riedel shears) that form during the initial stage of deformation, before the development of a throughgoing shear. The finite length of these oblique secondary fractures is of the same order of magnitude as the clay thickness.

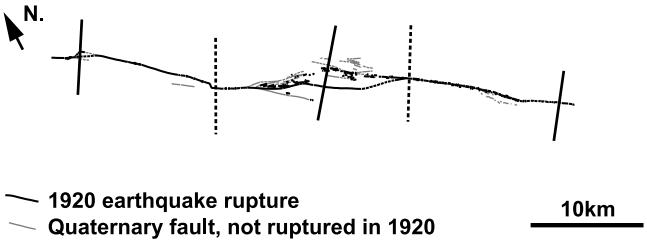

Figure 12. Example of fault geometry evolving through time along the Haiyuan fault, China. Quaternary faults are mapped in the field and local topography defines a typical pull-apart basin at this extensional step over. The bounds of the two segments that connect through the pull-apart are indicated by the vertical black lines. However, the 1920 Ms8 earthquake rupture went straight across the basin, suggesting that the segment geometry is evolving toward a new configuration, indicated by the dashed vertical lines, where bends would be moved both eastward and westward.

propagates in continental lithosphere [*Hubert-Ferrari et al.*, 2003]. Strike-slip faults, under these conditions, are observed to zigzag more than if they would form by simple interconnection of extensional cracks in a homogeneous medium.

[50] Smoothing of fault geometry has been documented, including during an earthquake [*Armijo et al.*, 2005], and is thought to result from surface roughness of faults being inversely related to their total displacement [*Wesnousky*, 1988; *Manighetti et al.*, 2007]. Such smoothing of a fault trace, however, is mainly of concern for large scale geometrical asperities, such as step overs of several kilometers or changes of azimuth of ten's of degrees [*Wesnousky*, 1988], and is not contradicted by our conclusion. Here we observed that segmentation, with a characteristic scale of ~21 km, could be identified on different faults that have accommodated various amount of total offset (Table 1). This suggests that if faults tend to smooth first-order geometric discontinuities with time and increasing total offset, some specific level of complexity in the fault trace persists at a smaller scale, making the fault zigzag around its average direction. Such complexity is interpreted to be directly related to some geometric control resulting from local crustal thickness. This has important implications when defining rupture scenarios, as such segments may or may not rupture in cascades during earthquakes [*Ward*, 1997; *Nielsen and Knopoff*, 1998; *Duan and Oglesby*, 2005]. Hence, knowing the characteristic size of segments narrows down the range of possible events and could help improve seismic hazard assessment in earthquake prone regions.

[51] The dynamic effects of a seismic rupture propagating along fault during an earthquake might explain the persistence of some level of complexity resulting in fault segmentation through successive earthquake cycles. Depending on the boundary conditions, if the earthquake rupture is propagating in a medium with pre-existing cracks that are oblique to the main fault, which is true in most cases, rupture might naturally branch on such secondary faults as a result of the dynamic stress build-up ahead of the rupture [*Poliakov et al.*, 2002; *Bhat et al.*, 2004]. Such an effect is likely to prevent the complete smoothing of the fault by recreating new complexity during each earthquake. As geometry does not evolve very quickly, a segment will remain similar through many seismic cycles, allowing geologists to observe growing jogs and bends along faults. When the fault reaches some critical threshold [*Duan and Oglesby*, 2006], however, in order to decrease complexity formed by growing relay zones, geometry would evolve and a new segment would propagate (Figure 12), resulting in a compromise between the regional stress field and the geometry of the neighboring fault segments.

[52] **Acknowledgments.** I thank G. King, P. Tapponnier, M. Ishii, and R. Dmowska for fruitful discussions and A. Nicol and C. Scholtz for constructive comments on an earlier version of this manuscript. This paper benefited from thoughtful reviews from the Assistant Editor, A. Agnon, T. Rockwell, and an anonymous reviewer. Figure 1 has been made possible thanks to P. Hellweg, who led me to original documents by J. C. Branner. This work was funded by CNRS, and I was supported by grant NSF-EAR Award 0440145 and Department of Earth and Planetary Sciences during my stay at Harvard University. This is IPGP contribution 2605.

References

Agnew, D. C., S. Owen, Z. K. Shen, G. Anderson, J. Svarc, H. Johnson, K. E. Austin, and R. Reilinger (2002), Coseismic displacements from the Hector Mine, California, earthquake: Results from survey-mode global positioning system measurements, *Bull. Seismol. Soc. Am.*, *92*(4), 1355–1364, doi:10.1785/0120000928.

Antolik, M., A. Kaverina, and D. S. Dreger (2000), Compound rupture of the great 1998 Antarctic plate earthquake, *J. Geophys. Res.*, *105*(B10), 23,825–23,838, doi:10.1029/2000JB900246.

Aochi, H., E. Fukuyama, and M. Matsu'ura (2000), Spontaneous rupture propagation on a non-planar fault in 3-D elastic medium, *Pure Appl. Geophys.*, *157*, 2003–2027, doi:10.1007/PL00001072.

Armijo, R., P. Tapponnier, and H. TongLin (1989), Late Cenozoic right-lateral faulting in southern China, *J. Geophys. Res.*, *94*(B3), 2787–2838, doi:10.1029/JB094iB03p02787.

Armijo, R., et al. (2005), Submarine fault scarps in the Sea of Marmara pull-apart (North Anatolian Fault): Implications for seismic hazard in Istanbul, *Geochem. Geophys. Geosyst.*, *6*, Q06009, doi:10.1029/2004GC000896.

Arrowsmith, J. R., and D. D. Rhodes (1994), Original forms and initial modifications of the Galway Lake road scarp formed along the Emerson fault during the 28 June 1992 Landers, California, earthquake, *Bull. Seismol. Soc. Am.*, *84*(3), 511–527.

Bayasgalan, A., J. Jackson, and D. McKenzie (2005), Lithosphere rheology and active tectonics in Mongolia: Relations between earthquake source parameters, gravity and GPS measurements, *Geophys. J. Int.*, *163*, 1151–1179, doi:10.1111/j.1365-246X.2005.02764.x.

Beanland, S., and M. Clark (1994), The Owens Valley fault zone, eastern California, and surface faulting associated with the 1872 earthquake, *U.S. Geol. Surv. Bull.*, *1982*, 29 p.

Berberian, M., J. Jackson, M. Qorashi, M. Khatib, K. Priestley, M. Telabian, and M. Ghafuri-Ashtiani (1999), The 1997 May 10 Zirkuh (Qa'enat) earthquake (M_w 7.2), Faulting along the Sistan suture zone of eastern Iran, *Geophys. J. Int.*, *136*, 671–694, doi:10.1046/j.1365-246x.1999.00762.x.

Beresnev, I. (2003), Uncertainties in finite-fault slip inversions: To what extent to believe? (a critical review), *Bull. Seismol. Soc. Am.*, *93*(6), 2445–2458, doi:10.1785/0120020225.

Bhat, H., R. Dmowska, J. Rice, and N. Kame (2004), Dynamic slip transfer from the Denali to Totschunda faults, Alaska: Testing theory for fault branching, *Bull. Seismol. Soc. Am.*, *94*(6B), S202–S213, doi:10.1785/0120040601.

Bhat, H. S., R. Dmowska, G. C. P. King, Y. Klinger, and J. R. Rice (2007), Off-fault damage patterns due to supershear ruptures with application to the 2001 M_w 8.1 Kokoxili (Kunlun) Tibet earthquake, *J. Geophys. Res.*, *112*, B06301, doi:10.1029/2006JB004425.

Bilham, R., and P. Williams (1985), Sawtooth segmentation and deformation processes on the southern San Andreas fault, California, *Geophys. Res. Lett.*, *12*, *557–560*, doi:10.1029/GL012i009p00557.

Boyd, S., and L. Vandenberghe (2004), *Convex Optimization*, Cambridge Univ. Press, Cambridge, U. K.

Calais, E., M. Vergnolle, V. San'kov, A. Lukhnev, A. Miroshnitchenko, S. Amarjargal, and J. Déverchère (2003), GPS measurements of crustal deformation in the Baikal-Mongolia area (1994–2002): Implications

for current kinematics of Asia, *J. Geophys. Res.*, *108*(B10), 2501, doi:10.1029/2002JB002373.

Chen, W. P., and P. Molnar (1983), Focal depths of intracontinental and intraplate earthquakes and their implications for the thermal and mechanical properties of the lithosphere, *J. Geophys. Res.*, *88*, 4183–4214, doi:10.1029/JB088iB05p04183.

Chen, J., D. J. Wald, and D. V. Helmberger (2002a), Source description of the 1999 Hector Mine, California, earthquake, Part I: Wavelet domain inversion theory and resolution analysis, *Bull. Seismol. Soc. Am.*, *92*(4), 1192–1207, doi:10.1785/0120000916.

Chen, J., D. J. Wald, and D. V. Helmberger (2002b), Source description of the 1999 Hector Mine, California, earthquake, Part II: Complexity of slip history, *Bull. Seismol. Soc. Am.*, *92*(4), 1208–1226, doi:10.1785/0120000917.

Chester, F. M., and J. S. Chester (1998), Ultracataclasite structure and friction processes of the Punchbowl fault, San Andreas system, California, *Tectonophysics*, *295*(1–2), 199–221, doi:10.1016/S0040-1951(98)00121-8.

Chu, R., L. Zhu, and D. Helmberger (2009), Determination of earthquake focal depths and source time functions in central Asia using teleseismic *P* waveforms, *Geophys. Res. Lett.*, *36*, L17317, doi:10.1029/2009GL039494.

Clévédé, E., M. P. Bouin, B. Bukchin, A. Mostinsky, and G. Patau (2004), New constraints on the rupture process of the 1999 August 17 Izmit earthquake deduced from estimates of stress glut rate moments, *Geophys. J. Int.*, *159*(3), 931–942, doi:10.1111/j.1365-246X.2004.02304.x.

Cotton, F., and M. Campillo (1995), Frequency domain inversion of strong ground motion: Application to the 1992 Landers earthquake, *J. Geophys. Res.*, *100*, 3961–3975, doi:10.1029/94JB02121.

Delouis, B., P. Lundgren, and D. Giardini (2004), Slip distributions of the 1999 Dücze (Mw 7.2) and Izmit (Mw 7.6) earthquakes on the North Anatolian Fault (Turkey): A combined analysis, report, Eidg. Tech. Hochsch., Zurich, Switzerland

Déverchère, J., C. Petit, N. Gileva, N. Radziminovitch, V. Melnikova, and V. San'kov (2001), Depth distribution of earthquakes in the Baikal rift system and its implications for the rheology of the lithosphere, *Geophys. J. Int.*, *146*, 714–730, doi:10.1046/j.0956-540x.2001.1484.484.x.

Duan, B., and D. D. Oglesby (2005), Multicycle dynamics of nonplanar strike-slip faults, *J. Geophys. Res.*, *110*, B03304, doi:10.1029/2004JB003298.

Duan, B., and D. D. Oglesby (2006), Heterogeneous fault stresses from previous earthquakes and the effect on dynamics of parallel strike-slip faults, *J. Geophys. Res.*, *111*, B05309, doi:10.1029/2005JB004138.

Duman, T., O. Emre, A. Dogan, and S. Ozalp (2005), Step-over and bend structures along the 1999 Duzce Earthquake surface rupture, North Anatolian fault, Turkey, *Bull. Seismol. Soc. Am.*, *95*(4), 1250–1262, doi:10.1785/0120040082.

Engdahl, E. R., J. A. Jackson, S. C. Myers, E. A. Bergman, and K. Priestley (2006), Relocation and assessment of seismicity in the Iran region, *Geophys. J. Int.*, *167*, 761–778, doi:10.1111/j.1365-246X.2006.03127.x.

Fliss, S., H. Bhat, R. Dmowska, and J. Rice (2005), Fault branching and rupture directivity, *J. Geophys. Res.*, *110*, B06312, doi:10.1029/2004JB003368.

Florensov, N. A., and V. P. Solonenko (1965), *The Gobi-Altai Earthquake*, 424 pp., U.S. Dep. of Commer., Washington, D. C.

Freymueller, J., N. E. King, and P. Segall (1994), The co-seismic slip distribution of the Landers earthquake, *Bull. Seismol. Soc. Am.*, *84*(3), 646–659.

Galgana, G., M. Hamburger, R. McCaffrey, E. Corpuz, and Q. Chen (2007), Analysis of crustal deformation in Luzon, Philippines using geodetic observations and earthquake focal mechanisms, *Tectonophysics*, *432*(1–4), 63–87, doi:10.1016/j.tecto.2006.12.001.

Graymer, R. W., V. E. Langenheim, R. W. Simpson, R. C. Jachens, and D. A. Ponce (2007), Relatively simple through-going fault planes at large-earthquake depth may be concealed by the surface complexity of strike-slip faults, *Geol. Soc. London Spec. Publ.*, *290*, 180–201, doi:10.1144/SP290.5

Haeussler, P. J., et al. (2004), Surface rupture and slip distribution of the Denali and Totschunda faults in the 3 November 2002 M 7.9 earthquake, Alaska, *Bull. Seismol. Soc. Am.*, *94*(6B), S23–S52, doi:10.1785/0120040626.

Harris, R., and S. Day (1993), Dynamics of fault interaction: Parallel strike-slip faults, *J. Geophys. Res.*, *98*(B3), 4461–4472, doi:10.1029/92JB02272.

Harris, R., and S. Day (1999), Dynamic 3D simulations of earthquakes on En Echelon Faults, *Geophys. Res. Lett.*, *26*(14), 2089–2092, doi:10.1029/1999GL900377.

Harris, R., R. Archuleta, and S. Day (1991), Fault steps and the dynamic rupture process: 2-D numerical simulations of a spontaneously propagating shear fracture, *Geophys. Res. Lett.*, *18*, 893–896, doi:10.1029/91GL01061.

Hartzell, S., P. Liu, C. Mendoza, C. Ji, and K. M. Larson (2007), Stability and uncertainty of finite-fault slip inversions: Application to the 2004 Parkfield, California, earthquake, *Bull. Seismol. Soc. Am.*, *97*(6), 1911–1934, doi:10.1785/0120070080.

Heermance, R., Z. K. Shipton, and J. P. Evans (2003), Fault structure control on fault slip and ground motion during the 1999 rupture of the Chelungpu fault, Taiwan, *Bull. Seismol. Soc. Am.*, *93*(3), 1034–1050, doi:10.1785/0120010230.

Hubert-Ferrari, A., G. C. P. King, I. Manighetti, R. Armijo, B. Meyer, and P. Tapponnier (2003), Long-term elasticity in the continental lithosphere; modeling the Aden Ridge propagation and the Anatolian extrusion process, *Geophys. J. Int.*, *153*(1), 111–132, doi:10.1046/j.1365-246X.2003.01872.x.

Hudnut, K. W., A. Borsa, C. Glennie, and J. B. Minster (2002), High-resolution topography along surface rupture of the 16 October 1999 Hector Mine, California, earthquake (M_w 7. 1) from airborne laser swath mapping, *Bull. Seismol. Soc. Am.*, *92*(4), 1570–1576, doi:10.1785/0120000934.

Institute of Geology (1990), *Active Haiyuan Fault Zone Monograph*, 286 pp., Seismol. Publ. House, Beijing, China.

Jachens, R. C., V. E. Langenheim, and J. C. Matti (2002), Relationship of the 1999 Hector Mine and 1992 Landers fault rupture to offsets on Neogene faults and distribution of late Cenozoic basins in the Eastern California shear zone, *Bull. Seismol. Soc. Am.*, *92*(4), 1592–1605, doi:10.1785/0120000915.

Johnson, A. M., R. W. Fleming, and K. M. Cruikshank (1994), Shear zones formed along long, straight traces of fault zones during the 28 June 1992 Landers, California, earthquake, *Bull. Seismol. Soc. Am.*, *84*(3), 499–510.

Karig, D. E. (1983), Accreted terranes in the northern part of the Philippine archipelago, *Tectonics*, *2*, 211–223, doi:10.1029/TC002i002p00211.

Kaverina, A., D. Dreger, and E. Price (2002), The combined inversion of seismic and geodetic data for the source process of the 16 October 1999 M_w 7.1 Hector Mine, California, earthquake, *Bull. Seismol. Soc. Am.*, *92*(4), 1266–1280, doi:10.1785/0120000907.

Kim, S.-J., K. Koh, S. Boyd, and D. Gorinevsky (2009), l1 trend filtering, *SIAM Rev.*, *51*(2), 339–360, doi:10.1137/070690274.

King, G. C. P. (1986), Speculations on the geometry of the initiation and termination processes of earthquake rupture and its relation to morphology and geological structures, *Pure Appl. Geophys.*, *124*(3), 567–585, doi:10.1007/BF00877216.

King, G. C., and J. Nabelek (1985), The role of fault bends in faults in the initiation and termination of earthquake rupture, *Science*, *228*, 984–987, doi:10.1126/science.228.4702.984.

King, G. C. P., and S. Wesnousky (2007), Scaling of fault parameters for continental strike-slip earthquakes, *Bull. Seismol. Soc. Am.*, *97*(6), 1833–1840, doi:10.1785/0120070048.

King, G., Y. Klinger, D. Bowman, and P. Tapponnier (2005), Slip-partitioned surface breaks for the 2001 Kokoxili earthquake, China (M_w 7.8), *Bull. Seismol. Soc. Am.*, *95*(2), 731–738, doi:10.1785/0120040101.

Klinger, Y., X. W. Xu, P. Tapponnier, J. Van der Woerd, C. Lasserre, and G. King (2005), High-resolution satellite imagery mapping of the surface rupture and slip distribution of the M_w 7.8, 14 November 2001 Kokoxili Earthquake, Kunlun Fault, northern Tibet, China, *Bull. Seismol. Soc. Am.*, *95*(5), 1970–1987, doi:10.1785/0120040233.

Klinger, Y., R. Michel, and G. C. P. King (2006), Evidence for an earthquake barrier model from Mw similar to 7.8 Kokoxili (Tibet) earthquake slip-distribution, *Earth Planet. Sci. Lett.*, *242*(3–4), 354–364, doi:10.1016/j.epsl.2005.12.003.

Knuepfer, P. L. K. (1989), Implication of the characteristics of end-points of historical surface ruptures for the nature of fault segmentation, *U.S. Geol. Surv. Open File Rep.*, *89-315*, 193–228.

Kurushin, R. A., A. Bayasgalan, M. Ölziybat, B. Enhtuvshin, P. Molnar, C. Bayarsayhan, K. Hudnut, and L. Jian (1997), The surface rupture of the 1957 Gobi-Altay, Mongolia, Earthquake, *Spec. Pap. Geol. Soc. Am.*, *320*, 142 p.

Lasserre, C., B. Bukchin, P. Bernard, P. Tapponnier, Y. Gaudemer, A. Mostinsky, and R. Dailu (2001), Source parameters and tectonic origin of the 1996 June 1 Tianzhu (M_w =5.2) and 1995 July 21 Yongden (M_w = 5.6) earthquakes near the Haiyuan fault (Gansu, China), *Geophys. J. Int.*, *144*(1), 206–220, doi:10.1046/j.1365-246x.2001.00313.x.

Lawson, A. C., et al. (1908), *The California Earthquake of April 18, 1906: Report of the State Earthquake Investigation Commission*, 451 pp., Carnegie Inst. of Wash., Washington, D.C.

Lee, W. H. K., H. Kanamori, P. C. Jennings, and C. Kisslinger (Eds.) (2002), *International Handbook of Earthquake and Engineering Seismology*, 925 pp., Academic, London.

Lettis, W., J. Bachhuber, R. Witter, C. Brankman, C. E. Randolph, A. Barka, W. Page, and A. Kaya (2002), Influence or releasing step-overs on surface

rupture and fault segmentation: Examples from the 17 August 1999 Izmit earthquake on the North Anatolia fault, Turkey, *Bull. Seismol. Soc. Am.*, *92*(1), 19–42, doi:10.1785/0120000808.

Li, Y.-G., J. E. Vidale, K. Aki, C. J. Marone, and W. H. K. Lee (1994), Fine structure of the Landers Fault Zone: Segmentation and the rupture process, *Science*, *265*, 367–370, doi:10.1126/science.265.5170.367.

Li, H. B., J. Van der Woerd, P. Tapponnier, Y. Klinger, X. X. Qi, J. S. Yang, and Y. T. Zhu (2005), Slip rate on the Kunlun fault at Hongshui Gou, and recurrence time of great events comparable to the 14/11/2001, Mw ~7.9 Kokoxili earthquake, *Earth Planet. Sci. Lett.*, *237*(1–2), 285–299.

Maggi, A., J. A. Jackson, D. McKenzie, and K. Priestley (2000), Earthquake focal depths, effective elastic thickness, and the strength of the continental lithosphere, *Geology*, *28*(6), 495–498, doi:10.1130/0091-7613(2000)28<495:EFDEET>2.0.CO;2.

Manighetti, I., M. Campillo, S. Bouley, and F. Cotton (2007), Earthquake scaling, fault segmentation, and structural maturity, *Earth Planet. Sci. Lett.*, *253*(3–4), 429–438, doi:10.1016/j.epsl.2006.11.004.

Mann, P. (2007), Global catalogue, classification and tectonic origins of retraining and releasing bends on active and ancient strike-slip fault systems, *Geol. Soc. London Spec. Pub.*, *290*, 13–142, doi:10.1144/SP290.2

McGill, S., and C. Rubin (1999), Surficial slip distribution on the central Emerson fault during the June 28, 1992, Landers earthquake, *J. Geophys. Res.*, *104*(B3), 4811–4833, doi:10.1029/98JB01556.

Mitchell, A. M., F. Hernandez, and J. R. Delacruz (1986), Cenozoic evolution of the Philippine Archipelago, *J. Southeast Asian Earth Sci.*, *1*, 3–22, doi:10.1016/0743-9547(86)90003-6.

Molnar, P., and W. P. Chen (1983), Focal depths and fault plane solutions of earthquakes under the Tibetan plateau, *J. Geophys. Res.*, *88*, 1180–1196, doi:10.1029/JB088iB02p01180.

Mooney, W. D., G. Laske, and G. Masters (1998), CRUST 5.1: A global crustal model at 5° × 5°, *J. Geophys. Res.*, *103*, 727–747, doi:10.1029/97JB02122.

Nakata, T., H. Tsutsumi, R. S. Punongbayan, R. E. Rimando, J. Daligdig, A. Daag, and G. M. Besana (1996), Surface fault ruptures of the 1990 Luzon earthquake, Philippines, *Spec. Publ. 25*, Res. Cent. for Regional Geogr., Hiroshima Univ., Hiroshima, Japan.

Nazareth, J. J., and E. Hauksson (2004), The seismogenic thickness of the southern California crust, *Bull. Seismol. Soc. Am.*, *94*(3), 940–960, doi:10.1785/0120020129.

Nielsen, S., and L. Knopoff (1998), The equivalent strength of geometrical barriers to earthquakes, *J. Geophys. Res.*, *103*(B5), 9953–9965, doi:10.1029/97JB03293.

Page, M. T., S. Custodio, R. J. Archuleta, and J. M. Carlson (2009), Constraining earthquake source inversion with GPS data: 1. Resolution-based removal of artifacts, *J. Geophys. Res.*, *114*, B01314, doi:10.1029/2007JB005449.

Pinet, N., and J. F. Stephan (1990), The Philippine wrench fault system in the Ilocos foothills, northwestern Luzon, Philippines, *Tectonophysics*, *183*, 207–224, doi:10.1016/0040-1951(90)90417-7.

Poliakov, A. N., R. Dmowska, and J. R. Rice (2002), Dynamic shear rupture interactions with fault bends and off-axis secondary faulting, *J. Geophys. Res.*, *107*(B11), 2295, doi:10.1029/2001JB000572

Replumaz, A., and P. Tapponnier (2003), Reconstruction of the deformed collision zone between India and Asia by backward motion of lithospheric blocks, *J. Geophys. Res.*, *108*(B6), 2285, doi:10.1029/2001JB000661

Schlische, R. W., M. O. Withjack, and G. Eisenstadt (2002), An experimental study of the secondary deformation produced by oblique-slip normal faulting, *AAPG Bull.*, *86*(5), 885–906.

Scholz, C. H. (1985), The Black Mountain asperity: Seismic hazard of the southern San Francisco peninsula, California, *Geophys. Res. Lett.*, *12*, 717–719, doi:10.1029/GL012i010p00717.

Scholz, C. (1990), *The Mechanics of Earthquakes and Faulting*, 439 pp., Cambridge Univ. Press, New York.

Scholz, C. (1998), A further note on earthquake size distributions, *Bull. Seismol. Soc. Am.*, *88*(5), 1325–1326.

Schwartz, D. P., and K. J. Coppersmith (1984), Fault behavior and characteristic earthquakes: Examples from the Wasatch and San Andreas fault zones, *J. Geophys. Res.*, *89*, 5681–5698, doi:10.1029/JB089iB07p05681.

Segall, P., and M. Lisowski (1990), Surface displacements in the 1906 San Francisco and 1989 Loma Prieta earthquakes, *Science*, *250*, 1241–1244, doi:10.1126/science.250.4985.1241.

Sharp, R. (1967), San Jacinto fault zone in the Peninsular Ranges of the southern California, *Geol. Soc. Am. Bull.*, *78*, 705–729, doi:10.1130/0016-7606(1967)78[705:SJFZIT]2.0.CO;2.

Sharp, R., et al. (1989), Surface faulting along the Superstition Hills fault zone and nearby faults associated with the earthquakes of 24 November 1987, *Bull. Seismol. Soc. Am.*, *79*, 252–281.

Sibson, R. (1985), Stopping of earthquake ruptures at dilational fault jogs, *Nature*, *316*, 248–251, doi:10.1038/316248a0.

Sibson, R. H. (2003), Thickness of the seismic slip zone, *Bull. Seismol. Soc. Am.*, *93*(3), 1169–1178, doi:10.1785/0120020061.

Sieh, K. (1996), The repetition of large-earthquake ruptures, *Proc. Natl. Acad. Sci. U. S. A.*, *93*, 3764–3771, doi:10.1073/pnas.93.9.3764.

Sieh, K., et al. (1993), Near-field investigations of the Landers earthquake sequence, April to July 1992, *Science*, *260*, 171–176, doi:10.1126/science.260.5105.171.

Simons, M., Y. Fialko, and L. Rivera (2002), Coseismic deformation from the 1999 M_w 7.1 Hector Mine, California, earthquake as inferred from InSAR and GPS observations, *Bull. Seismol. Soc. Am.*, *92*(4), 1390–1402, doi:10.1785/0120000933.

Sowers, J., J. R. Unruh, W. Lettis, and T. D. Rubin (1994), Relationship of the Kickapoo fault to the Johnson Valley and Homestead Valley faults, San Bernardino County, California, *Bull. Seismol. Soc. Am.*, *84*, 528–536.

Spotila, J., and K. Sieh (1995), Geologic investigations of a "slip gap" in the surficial ruptures of the 1992 Landers earthquake, southern California, *J. Geophys. Res.*, *100*(B1), 543–559, doi:10.1029/94JB02471.

Stirling, M., S. Wesnousky, and K. Shimazaki (1996), Fault trace complexity, cumulative slip, and the shape of the magnitude-frequency distribution for strike-slip faults: A global survey, *Geophys. J. Int.*, *124*, 833–868, doi:10.1111/j.1365-246X.1996.tb05641.x.

Sudhaus, H., and S. Jonsson (2009), Improved source modelling through combined use of InSAR and GPS under consideration of correlated data errors: Application to the June 2000 Kleifarvatn earthquake, Iceland, *Geophys. J. Int.*, *176*(2), 389–404, doi:10.1111/j.1365-246X.2008.03989.x.

Thatcher, W., G. Marshall, and M. Lisowski (1997), Resolution of fault slip along the 470-km-long rupture of the great 1906 San Francisco earthquake and its implications, *J. Geophys. Res.*, *102*(B3), 5353–5367, doi:10.1029/96JB03486.

Treiman, J. A., et al. (2002), Primary surface rupture associated with the M_w 7.1 16 October 1999 Hector Mine earthquake, San Bernardino County, Californian, *Bull. Seismol. Soc. Am.*, *92*(4), 1171–1191, doi:10.1785/0120000923.

Vallée, M., and M. Bouchon (2004), Imaging coseismic rupture in far field by slip patches, *Geophys. J. Int.*, *156*(3), 615–630, doi:10.1111/j.1365-246X.2004.02158.x.

Vallée, M., M. Landès, N. M. Shapiro, and Y. Klinger (2008), The 14 November 2001 Kokoxili (Tibet) earthquake: High-frequency seismic radiation originating from the transition between sub-Rayleigh and supershear rupture velocity regimes, *J. Geophys. Res.*, *113*, B07305, doi:10.1029/2007JB005520.

Van Der Woerd, J., P. Tapponnier, F. J. Ryerson, A. S. Meriaux, B. Meyer, Y. Gaudemer, R. C. Finkel, M. W. Caffee, G. G. Zhao, and Z. Q. Xu (2002), Uniform postglacial slip-rate along the central 600 km of the Kunlun Fault (Tibet), from Al-26, Be-10, and C-14 dating of riser offsets, and climatic origin of the regional morphology, *Geophys. J. Int.*, *148*(3), 356–388, doi:10.1046/j.1365-246x.2002.01556.x.

Wald, D., and T. Heaton (1994), Spatial and temporal distribution of slip for the 1992 Landers, California, earthquake, *Bull. Seismol. Soc. Am.*, *84*(3), 668–691.

Walker, R., J. Jackson, and C. Baker (2004), Active faulting and seismicity of the Dasht-e-Bayaz region, eastern Iran, *Geophys. J. Int.*, *157*(1), 265–282, doi:10.1111/j.1365-2966.2004.02179.x

Wallace, R. E. (1973), Surface fracture patterns along the San Andreas fault, paper presented at Tectonic Problems of the San Andreas Fault System, Stanford Univ., Palo Alto, Calif.

Wallace, R. E. (1989), Segmentation in fault zones, in *Proceedings of Conference XLV Fault Segmentation and Controls of Rupture Initiation and Termination*, edited by D. P. Schwartz and R. H. Sibson, *U.S. Geol. Surv. Open File Rep., 89-315*.

Ward, S. (1997), Dogtails versus rainbows: Synthetic earthquake rupture models as an aid in interpreting geological data, *Bull. Seismol. Soc. Am.*, *87*, 1422–1441.

Weldon, R., T. Fumal, and G. P. Biasi (2004), Wrightwood and the earthquake cycle: What a long recurrence record tells us about how faults work, *GSA Today*, *14*(9), 4–10, doi:10.1130/1052-5173(2004)014<4:WATECW>2.0.CO;2.

Wesnousky, S. G. (1988), Seismological and structural evolution of strike-slip faults, *Nature*, *335*(22), 340–343, doi:10.1038/335340a0.

Wesnousky, S. (2006), Predicting the endpoints of earthquake ruptures, *Nature*, *444*(7117), 358–360, doi:10.1038/nature05275.

Wibberley, C. A. J., and T. Shimamoto (2003), Internal structure and permeability of major strike-slip fault zones: The Median Tectonic Line in Mie Prefecture, Southwest Japan, *J. Struct. Geol.*, *25*(1), 59–78, doi:10.1016/S0191-8141(02)00014-7.

Xu, X., W. Chen, W. Ma, G. Yu, and G. Chen (2002), Surface rupture of the Kunlunshan earthquake (Ms 8.1), northern Tibetan plateau, China, *Seismol. Res. Lett.*, *73*(6), 884–892.

Xu, X. W., G. H. Yu, Y. Klinger, P. Tapponnier, and J. Van der Woerd (2006), Reevaluation of surface rupture parameters and faulting segmentation of the 2001 Kunlunshan earthquake (M_w 7.8), northern Tibetan Plateau, China, *J. Geophys. Res.*, *111*, B05316, doi:10.1029/2004JB003488.

Yang, Z. X., F. Waldhauser, Y. T. Chen, and P. G. Richards (2005), Double-difference relocation of earthquakes in central-western China, 1992–1999, *J. Seismol.*, *9*, 241–264, doi:10.1007/s10950-005-3988-z.

Yoshida, Y., and K. Abe (1992), Source mechanism of the Luzon, Philippines earthquake of July 16, 1990, *Geophys. Res. Lett.*, *19*(6), 545–548, doi:10.1029/91GL02467.

Zachariasen, J., and K. Sieh (1995), The transfer of slip between two en echelon strike-slip faults: A case-study from the 1992 Landers earthquake, southern California, *J. Geophys. Res.*, *100*(B8), 15,281–15,301, doi:10.1029/95JB00918.

Zhang, W., D. Jiao, P. Zhang, P. Molnar, B. C. Burchfield, Q. Deng, Y. Wang, and F. Song (1987), Displacement along the Haiyuan fault associated with the great 1920 Haiyuan, China, earthquake, *Bull. Seismol. Soc. Am.*, *77*(1), 117–131.

Zhou, S. Y., K. Irikura, and X. F. Chen (2004), Analysis of the reliability and resolution of the earthquake source history inferred from waveforms, taking the Chi-Chi earthquake as an example, *Geophys. J. Int.*, *157*(3), 1217–1232, doi:10.1111/j.1365-246X.2004.02247.x.

Y. Klinger, Institut de Physique du Globe Paris, CNRS, 4, pl. Jussieu, Boite 89, F-75005 Paris CEDEX 05, France. (klinger@ipgp.jussieu.fr)